Hail Parameter Relations: A Comprehensive Digest

CARLTON W. ULBRICH

Department of Physics and Astronomy, Clemson University, Clemson, SC 29631

DAVID ATLAS

Laboratory for Atmospheric Sciences, NASA Goddard Space Flight Center, Greenbelt, MD 20771

(Manuscript received 10 October 1980, in final form 13 September 1981)

ABSTRACT

Diagrams are presented which display the relationships between hailstone size distribution parameters and integral quantities defined in terms of these parameters. It is assumed that the hailstones are spherical and homogeneous, are distributed with respect to size according to a truncated exponential distribution, and that they fall in still air without rain. Some of the diagrams are shown to have application for size distributions other than exponential provided that the moments of the distribution are known. Hailfall-related integral quantities depicted are the total number of hailstones per unit volume, liquid water content, kinetic energy content, fluxes of mass and kinetic energy, median volume diameter, average diameter, mass-weighted average diameter, variance of the size distribution, and number of hailstones greater than a specified minimum diameter.

Radar measurables are calculated using backscattering cross sections for spherical hailstones that are dry or coated with a thin film of liquid water of thickness t. The results are displayed on overlays for the hail parameter diagram for radar wavelengths of 3.21 cm and 10.0 cm for dry ($t = 0.0$) and wet ($t = 0.01$ cm) hail. Radar quantities shown on these overlays include the equivalent radar reflectivity factor, the mean Doppler fallspeed, the variance of the Doppler spectrum, and the ratio of the reflectivity factors for the above two radar wavelengths.

Applications of the diagram are presented, one of which uses experimental hail parameters of several investigators. Another involves analysis of 1976 National Hail Research Experiment hailpad data and the results are plotted on the diagram. Empirical results deduced from these analyses are used to construct a second form of hail parameter diagram which is convenient for analyzing possible effects due to natural or artificial modification of the hail size distribution. Experimental hail parameters are also plotted on this diagram and empirical equations are derived from these data to illustrate the relationships implied by such empirical analyses between all pairs of hail parameters. These results also are used to assess the error introduced by neglect of the contribution to remote measurables due to rain.

1. Introduction

After two decades of worldwide, sporadic collection of data on the numbers and sizes of hailstones, enough information has been accumulated to provide reasonable approximations to typical hail size distributions. In this work this information is used to develop theoretical and empirical relationships between the parameters of the distribution and a variety of physical quantities dependent thereon. Of particular interest are integral quantities such as total number concentration of hailstones, concentration above specific sizes, mass per unit volume, mass flux, kinetic energy content and kinetic energy flux; all of which are related to problems of damage by hailfall, to hail suppression, to methods of measurement of hail, and to parameterization of hail growth by modelers. Additional work presented here relates the characteristics of the hail spectrum to several radar measurables, such as equivalent radar reflectivity factor, mean Doppler fallspeed and variance of the Doppler spectrum, all at two commonly used wavelengths. The motivation for the latter is to determine how to measure best the physical properties of hail by radar and the limitations of such methods. All the hail properties are presented in a generalized hail parameter diagram comprised of a base diagram and a series of overlays which permit easy determination of any of the desired quantities from knowledge of a sufficient set of the others.

The theoretical calculations presented here assume that the size spectrum can be represented by a form which involves three parameters. Such an assumption means that to specify completely the size distribution requires knowledge of three quantities, such as the total number of hailstones per unit volume, a representative hailstone diameter (e.g., the average diameter), and the breadth of the distribution. The mathematical form of the distribution used here is a truncated exponential form i.e.,

$$N(D) = N_0 e^{-\Lambda D} (0 \leq D \leq D_{\max}), \qquad (1)$$

0021-8952/82/010022-22$09.50

where $N(D)$ (m^{-3} cm^{-1}) is the number of hailstones per unit volume per unit size interval and D (cm) is the hailstone diameter. With $N(D)$ having this form, the three quantities required to specify the distribution are the parameters N_0 (m^{-3} cm^{-1}), Λ (cm^{-1}) and the maximum hailstone diameter D_{max} (cm).

The assumption of an exponential distribution in Eq. (1) is supported by the observations of Douglas (1963) and Federer and Waldvogel (1975, 1978) at the surface and by the analysis of Doppler radar spectra of hail aloft by Ulbrich (1974, 1977). The reasons that the distribution must be truncated at a maximum diameter D_{max} have been discussed by Ulbrich (1977). Among these reasons are the physical arguments of Dennis and Musil (1973) who show that the most strongly correlated experimental hailstorm parameters are the maximum hailstone diameter, the maximum updraft velocity and the temperature of the updraft, therefore suggesting that a storm is capable of producing hailstones with diameters up to that which can be supported by the maximum updraft velocity. Furthermore, since much of the discussion in this work is concerned with remote measurement of hail parameters by radar and the contributing region of the radar beam is of finite size, the spectrum observed by radar will contain hailstones with diameters up to a maximum size which depends on the location in the storm as well as the time of observation during the lifetime of the storm. Nevertheless, in spite of the evidence in support of the specific form of $N(D)$ used to construct the diagrams in this work, it will be shown in a future publication that the results presented here have general applicability for arbitrary size distributions for which the moments of the distribution have been determined. This means that the diagrams can be used to examine the relationships among hail parameters for distributions of any form. It is only necessary that the moments of the distribution be given and these could be found empirically or theoretically.

It is recognized here that an instantaneous or short interval hail sample rarely produces a perfect truncated exponential distribution, although the 30 s time-resolved samples of Federer and Waldvogel (1978) are remarkably well approximated by exponentials as are those deduced by Ulbrich (1974) from short-interval measurements of Doppler spectra. Sampling considerations suggest that short-term deviations are to be expected (Gertzman and Atlas, 1978) and that it is some longer-term average spectrum which should be used. Large differences from exponentiality also are characteristic of short-interval raindrop spectra. Indeed, it was only by averaging a large set of drop-size spectra that Marshall and Palmer (1948) were able to arrive at the classical exponential distribution of raindrop sizes. Even then they noted that the exponential law does not fit well at small drop sizes, and there is a wide body of evidence of both statistical and physical deviations therefrom. Nevertheless, the Marshall and Palmer (1948) spectrum has long been used very effectively for a wide variety of scientific purposes. It is in the same spirit that the exponential distribution is used in this work.

Another very important assumption involved in this work is that the remote radar measurables represented on the diagrams include only the contribution due to hail, with the part due to rain considered negligible. This condition generally will be met when the rain contribution to the reflectivity factor is <10–20% of the total, but the existence of this condition is not always readily determined. In any case, it is important to isolate the radar characteristics of hail when the above requirement is met, for this will subsequently permit assessment of the limitations of the measurements when it is not met. The separation of the hail and rain parts of remote measurables probably requires measurement of more than two quantities as well as the use of specialized methods of analysis. This remains a major, unsolved problem in radar meteorology and will not be addressed in this work. However, the effect of neglecting the rain part of the reflectivity factor on the usefulness of the results presented in this work will be considered in detail in Section 3.

Two forms of hail parameter diagram are presented here. The first form is a three-parameter diagram and is general in that no assumptions are made about any relationships among the three distribution parameters N_0, Λ, and D_{max}. The second form of hail parameter diagram uses an empirically deduced relationship between Λ and D_{max} which considerably simplifies the presentation, transforms the diagram to a two-parameter form and makes it analogous to the diagram for rain presented by Ulbrich and Atlas (1978). Both forms consist of base diagrams supplemented by overlays. The base diagrams display the relationships among those quantities which are dependent only on the size distribution parameters and which are independent of any other quantities such as radar wavelength. The overlays are used with the base diagrams to depict the dependence of quantities such as radar reflectivity on all other quantities. Applications of both forms of diagrams are presented which use radar data and surface hailpad data of several workers. In addition, an analysis of 1976 National Hail Research Experiment hailpad data is performed and the results displayed on the hail parameter diagram.

2. Three-parameter diagram

a. Base diagram

In terms of the distribution parameters N_0, Λ and D_{max}, the definitions of some of the quantities of interest in this work are as follows: the liquid water

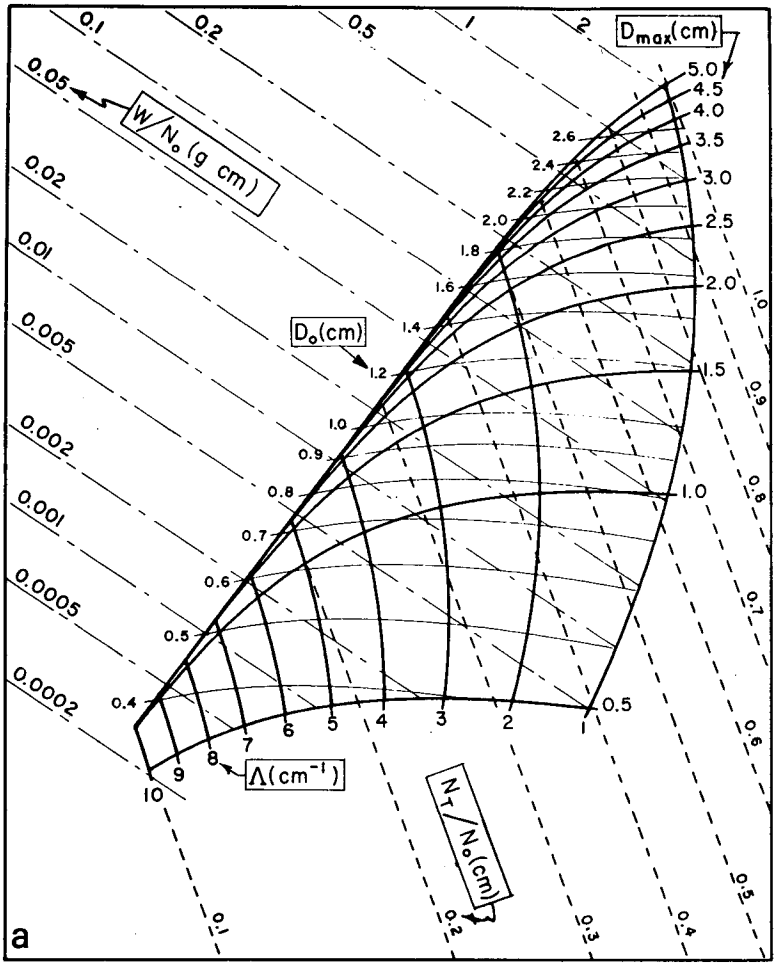

FIG. 1a. Three-parameter base diagram. Isopleths of W/N_0, N_T/N_0, Λ, D_{max} and D_0 are shown as light dot-dashed lines, dashed lines, heavy solid curves concave to left, heavy solid curves concave downward, and light solid curves, respectively. The units of the labels on the isopleths are shown on the diagram.

content W (g m^{-3}) is given by

$$W = \frac{\pi}{6}\rho \int_0^{D_{max}} D^3 N(D) dD = \frac{\pi \rho N_0}{6\Lambda^4} \Gamma(4, \Lambda D_{max}) \quad (2)$$

and the total number concentration of hailstones N_T (m^{-3}) is

$$N_T = \int_0^{D_{max}} N(D) dD = \frac{N_0}{\Lambda} \Gamma(1, \Lambda D_{max}). \quad (3)$$

In the above, $\Gamma(a, x)$ is the incomplete gamma function

$$\Gamma(a, x) = \int_0^x u^{a-1} e^{-u} du, \quad (4)$$

which approaches the limiting value $\Gamma(a, \infty) = (a - 1)!$ when $x \to \infty$. In addition, the hailstones have been assumed to be spherically homogeneous with mass density ρ (g cm^{-3}); in this work it will be assumed that $\rho = 0.9$ g cm^{-3}. Another commonly used parameter is the median volume diameter D_0 (cm) defined by

$$2 \int_0^{D_0} D^3 N(D) dD = \int_0^{D_{max}} D^3 N(D) dD. \quad (5)$$

Using Eq. (1), it is therefore found that D_0 is related to Λ and D_{max} through the relation

$$\Gamma(4, \Lambda D_0) = 0.5\Gamma(4, \Lambda D_{max}). \quad (6)$$

Consequently, the product ΛD_0 is determined solely by ΛD_{max} and, as shown by Atlas (1953), when $\Lambda D_{max} \to \infty$, $\Lambda D_0 \to 3.672$. The quantity ΛD_0 is within 5% of the latter value when $\Lambda D_{max} \geq 7$.

The relationships among N_T, W, N_0, Λ, D_{max} and D_0 are displayed graphically on the diagram in Fig. 1a. The diagram consists of a plot of W/N_0 *vs* N_T/N_0 with isopleths of D_{max} (heavy solid curves concave downward and to the right), Λ (heavy solid curves concave toward the left), and D_0 (light solid curves

concave downward). The vertical and horizontal axes are both skewed in the diagram so that isopleths of N_T/N_0 and W/N_0 are shown as light dashed lines and light dot-dashed lines, respectively. Since the units of N_T and W are m^{-3} and g m^{-3}, respectively, and the units of N_0 are m^{-3} cm^{-1}, then the labels on the N_T/N_0 isopleths are in centimeters and those on the W/N_0 isopleths are in g cm. The labels on the D_{max} isopleths are in cm and appear along the right boundary, those on the D_0 isopleths also are in centimeters and appear along the left boundary, and those on the Λ isopleths are in cm^{-1} and are shown below the bottom boundary. The ranges of label values have been chosen to span most of the experimentally observed values.

All of the isopleths in the diagram in Fig. 1a are dependent solely on the parameters Λ and D_{max} with the third parameter N_0 appearing as a normalizing divisor in W/N_0 and N_T/N_0. The diagram will therefore be referred to in this work as the *base diagram* since it depends on the size distribution parameters only and is independent of any other relationships describing the particle properties, e.g., the hailstone fallspeed law, the backscattering cross sections, etc. Several other quantities can be defined which also are dependent only on Λ and D_{max} and some of these are the average diameter $\bar{D}$ (cm) given by

$$\bar{D} = \frac{\int_0^{D_{max}} DN(D)dD}{\int_0^{D_{max}} N(D)dD} = \frac{1}{\Lambda}\frac{\Gamma(2, \Lambda D_{max})}{\Gamma(1, \Lambda D_{max})}, \quad (7)$$

the mass-weighted average diameter $\bar{D}_m$ (cm) defined as

$$\bar{D}_m = \frac{\int_0^{D_{max}} D^4N(D)dD}{\int_0^{D_{max}} D^3N(D)dD} = \frac{1}{\Lambda}\frac{\Gamma(5, \Lambda D_{max})}{\Gamma(4, \Lambda D_{max})} \quad (8)$$

and the variance of the distribution σ^2 (cm^2) defined by

$$\sigma^2 = \frac{\int_0^{D_{max}} (D - \bar{D})^2N(D)dD}{\int_0^{D_{max}} N(D)dD}$$

$$= \frac{1}{\Lambda^2}\left\{\left[\frac{\Gamma(3, \Lambda D_{max})}{\Gamma(1, \Lambda D_{max})}\right] - \left[\frac{\Gamma(2, \Lambda D_{max})}{\Gamma(1, \Lambda D_{max})}\right]^2\right\}. \quad (9)$$

Isopleths of $\bar{D}$, $\bar{D}_m$, σ^2 and the product ΛD_{max} are shown in Fig. 1b which can be used as an overlay of Fig. 1a.

Many other overlays similar to that shown above can be constructed which display the relationships of the quantities of interest to the size distribution

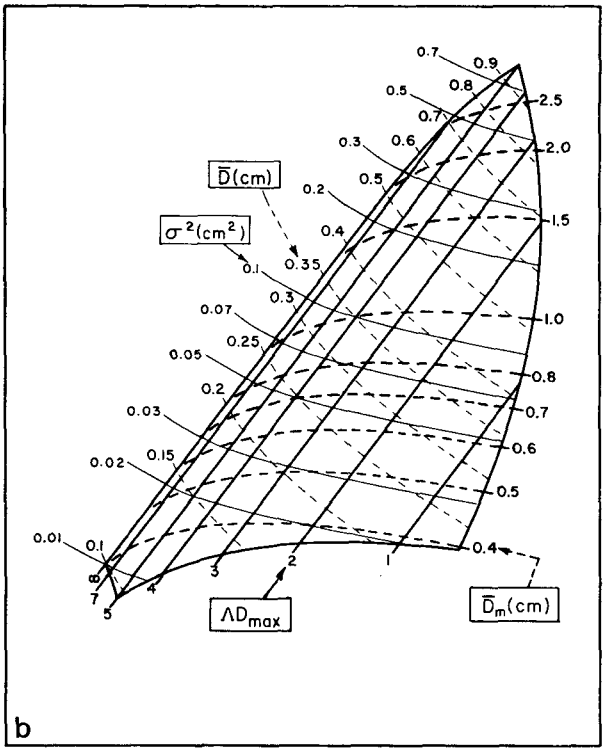

FIG. 1b. Supplement to three-parameter base diagram showing isopleths of $\bar{D}$, $\bar{D}_m$, ΛD_{max} and σ^2 as light dashed curves, heavy dashed curves, heavy straight lines, and light solid curves, respectively. The units of the labels on the isopleths are shown on the diagram.

parameters. For example, quantities which have been hypothesized as being related to the physical damage caused by hailfall are the kinetic energy content E (J m^{-3}) given by

$$E = \frac{1}{2}\int_0^{D_{max}} \frac{\pi}{6}\rho D^3v^2(D)N(D)dD$$

$$= \frac{0.001\pi\rho\gamma^2}{12\Lambda^5} N_0\Gamma(5, \Lambda D_{max}), \quad (10)$$

the kinetic energy flux $\dot{E}$ (J m^{-2} s^{-1}) defined as

$$\dot{E} = \frac{1}{2}\int_0^{D_{max}} \frac{\pi}{6}\rho D^3v^3(D)N(D)dD$$

$$= \frac{0.001\pi\rho\gamma^3}{12\Lambda^{5.5}} N_0\Gamma(5.5, \Lambda D_{max}) \quad (11)$$

and the mass flux $\dot{W}$ (g m^{-2} s^{-1}) defined by

$$\dot{W} = \int_0^{D_{max}} \frac{\pi}{6}\rho D^3v(D)N(D)dD$$

$$= \frac{\pi\rho\gamma}{6\Lambda^{4.5}} N_0\Gamma(4.5, \Lambda D_{max}). \quad (12)$$

An overlay depicting isopleths of E/N_0, $\dot{E}/N_0$ and $\dot{W}/N_0$ is not shown here since these isopleths are

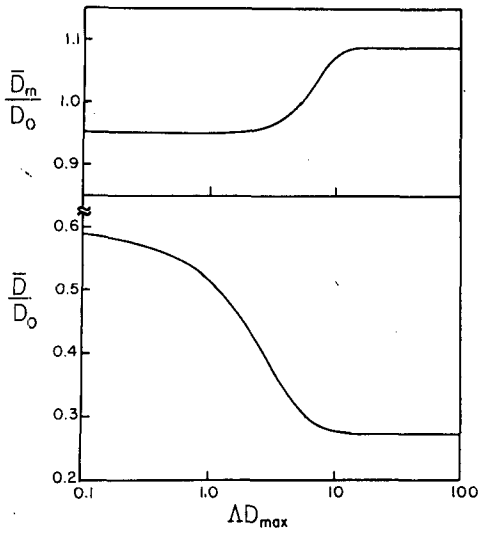

FIG. 2. The ratios $\bar{D}/D_0$ and $\bar{D}_m/D_0$ as functions of ΛD_{max}.

similar to those for W/N_0 in Fig. 1a. However, these damage-related quantities will be discussed further in the next section.

In Eq. (10)–(12) it has been assumed that the hailstones are falling in still air and therefore no account has been taken of the presence of vertical or horizontal winds. $\dot{E}$ and $\dot{W}$ might therefore be appropriately called the "intrinsic" *vertical* fluxes of kinetic energy and mass. Also, it has been assumed in the above that the fallspeeds of the hailstones can be approximated by

$$v(D) = \left(\frac{4\rho g}{3\rho_a C_D}\right)^{1/2} \sqrt{D} = \gamma\sqrt{D}, \qquad (13)$$

where $\rho = 0.9$ g cm^{-3} is the mass density of ice, $g = 9.8$ m s^{-2} is the acceleration due to gravity, ρ_a (g cm^{-3}) is the mass density of the air through which the hailstones are falling, and C_D is the drag coefficient. As reviewed by English (1973), the coefficient γ depends on several factors, such as the pressure and temperature of the air, and the shape and surface roughness of the hailstones. As in Waldvogel *et al.* (1978a), the value used in this work is $\gamma = 13.96$ m s^{-1} cm$^{-1/2}$ corresponding to $v(D)$ in m s^{-1} and D in cm. This value is appropriate to smooth, spherical hailstones falling in air with density equal to that for average conditions on the high plains of North America. For other values of γ the diagrams in this work can be adjusted by multiplying the labels on the isopleths by the appropriate constant factor. The only isopleths affected by such an adjustment will be those presented in the next section for E/N_0, $\dot{E}/N_0$, and $\dot{W}/N_0$.

In the above diagrams the W/N_0 and N_T/N_0 axes have been skewed at angles chosen such that the separation between the ΛD_{max} isopleths is a maximum, thereby clearly displaying the sensitivity of the hail parameters to changes in Λ and D_{max} and/or D_0. For example, the diagram in Fig. 1a demonstrates that N_T/N_0 is not very sensitive to variations in D_{max} along an isopleth of Λ over the entire range of the diagram, whereas W/N_0 is much more sensitive to such variations. As a specific example, for $\Lambda = 1$ cm^{-1}, N_T/N_0 decreases by about a factor of 2 when D_{max} varies from 5.0 to 0.5 cm, but for the same variation in D_{max}, W/N_0 decreases by almost three orders of magnitude. For $\Lambda \geq 4$ cm^{-1} the change in N_T/N_0 for the same variation in D_{max} is $< \sim 10\%$ but the change in W/N_0 is still large, amounting to almost an order of magnitude in some cases. These variations would not have been perceived had the W/N_0 and N_T/N_0 axes not been skewed. In fact, with rectangular axes all of the region of the diagram in Fig. 1a bounded by the $\Lambda = 1.0$ cm^{-1}, $\Lambda = 10.0$ cm^{-1}, $D_{max} = 0.5$ cm and $D_{max} = 5.0$ cm isopleths would be crowded so closely together that it would be difficult to detect changes in W/N_0 and N_T/N_0 due to variations in either Λ or D_{max}.

Inspection of Fig. 1b when overlaid on Fig. 1a shows that isopleths of $\bar{D}_m$ are quite similar to those of D_0 whereas isopleths of $\bar{D}$ are not at all like those of either D_0 or $\bar{D}_m$. In other words, the isopleths of $\bar{D}_m$ and D_0 are essentially parallel so that these two spectral parameters are practically identical over the full range of values of Λ and D_{max} spanned by the diagram. To illustrate this another way, the ratios $\bar{D}/D_0$ and $\bar{D}_m/D_0$ have been calculated from Eqs. (6)–(8). These ratios are dependent solely on the product ΛD_{max} and are plotted in Fig. 2 over the interval $0.1 \leq \Lambda D_{max} \leq 100$. It is seen from this figure that $\bar{D}_m$ is always within 10% of D_0, whereas $\bar{D}/D_0$ varies by more than a factor of 2. This result is particularly important in connection with the analysis of hail size spectral data since $\bar{D}_m$ is a more conveniently calculated quantity than D_0. In addition, the result found for $\bar{D}_m$ from experimental data would be statistically more representative than $\bar{D}$. This occurs because in calculating $\bar{D}_m$ the diameter is weighted according to the mass of the hailstone which therefore places greater emphasis on the range of diameters in the center of the spectrum near D_0, whereas computation of $\bar{D}$ places greater emphasis on the part of the spectrum with small diameters and large numbers of hailstones. This means that hailstone measurement methods which cannot detect hailstones with diameters less than a minimum diameter will still produce statistically meaningful results for $\bar{D}_m$ since the small diameter hailstones contribute little to the computation of this spectral parameter. These results are evident in the analysis of hailstone size distributions described by Weber (1976).

Many more comparisons of this type are possible; there are far too many to describe all of them in this

work. One interesting application of the diagram is shown in Fig. 3 where the results of several workers are displayed for experimentally-determined hail-size distribution parameters. For clarity only the isopleths of Λ, D_0 and ΛD_{max} are shown and they are unlabeled but can be identified easily by comparison with Figs. 1a and 1b. The triangles represent the results of Federer and Waldvogel (1975) for time-resolved hailstone size spectra measured on a hail platform in Switzerland, the diamond corresponds to the average of 67 hail spectra measured in Canada by Douglas (1963), the asterisks are hail spectra determined by Atlas and Ludlam (1960) for two storms in England, and the cross represents the average of spectra for three storms measured in Kenya by Rinehart (1975). Each of these data points was plotted using the values of Λ and D_{max} determined from the hailstone distribution measured at the surface. Also, shown in Fig. 3 as squares, are the results obtained by Ulbrich (1977) using the Doppler radar spectra measured aloft by Battan and Theiss (1972). These points were plotted using the values of D_0 and D_{max} deduced from the Doppler radar measurements. The procedure by which these parameters are found from the radar data is detailed by Ulbrich (1977). All of these results lie within a narrow region of the diagram near the left boundary in the region for $\Lambda D_{max} > 5$ which suggests that for most hail spectra the product ΛD_{max} can be assumed large. It has been shown by Ulbrich (1974, 1977) that such an assumption considerably simplifies the analysis of Doppler radar spectra of hail and removes the ambiguities inherent in such analyses. In the next section this result will be used to construct an alternative form of hail parameter diagram.

One of the advantages of using N_0 as a normalizing divisor in the base diagram is that it permits display of hail parameters as determined by hailpads when the time duration of hailfall is not known. Such data consist of numbers of hailstones $n(D_i)$ hitting the pad within a diameter category of width ΔD_i and with central diameter D_i. If the fallspeeds of the hailstones are assumed to have the form of Eq. (13), then the volume distribution of hailstones $N(D_i)$ above the hailpad is found from

$$N(D_i) = \frac{n(D_i)}{Av(D_i)\Delta t \Delta D_i} = \frac{n(D_i)}{\gamma A \Delta t D_i^{1/2} \Delta D_i}, \quad (14)$$

where A is the area of the hailpad and Δt is the time duration of hailfall. When an exponential distribution of the form of Eq. (1) is fitted to the data defined by Eq. (14), the result found for Λ will not depend on the constants γ, A or Δt but N_0 will be inversely proportional to the product $\gamma A \Delta t$. Consequently, hailpad data can be plotted on the hail parameter diagram by several different methods all of which do not require knowledge of Δt. For example, the

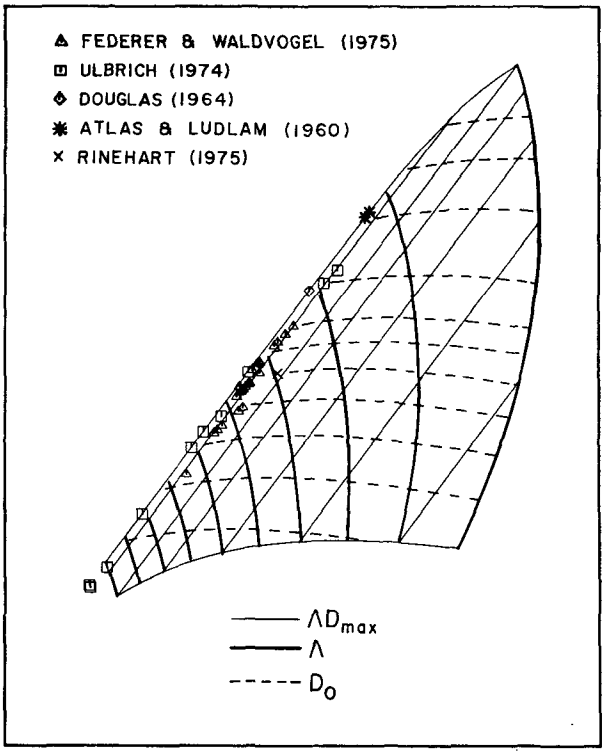

FIG. 3. Experimental hail parameters of several workers plotted on the three-parameter base diagram. See text for further details.

parameter Λ can be determined by plotting the hailpad data semi-logarithmically and estimating Λ from the slope of the resultant straight line. This value of Λ together with the value of the maximum hailstone diameter D_{max} define a point which can be plotted on the diagram. Another method involves computing W and N_T from the equations

$$W = \frac{\pi}{6} \rho \sum_i D_i^3 N(D_i) \Delta D_i \quad (15)$$

and

$$N_T = \sum_i N(D_i) \Delta D_i . \quad (16)$$

The ratio W/N_T is then independent of Δt and the exponential approximation to this ratio formed from Eqs. (2) and (3) is independent of N_0 and dependent only on Λ and the product ΛD_{max}. That is, Eqs. (2) and (3) yield

$$\frac{W}{N_T} = \frac{\pi \rho}{6} \frac{1}{\Lambda^3} \frac{\Gamma(4, \Lambda D_{max})}{\Gamma(1, \Lambda D_{max})} . \quad (17)$$

With Λ again estimated from the slope of a plot of $\ln N(D_i)$ vs D_i, Eq. (17) becomes an equation for the product ΛD_{max}. Its solution therefore produces a datum on the diagram defined by the two parameters Λ and ΛD_{max}. The advantage of this method is that it avoids the sampling problems inherent in estima-

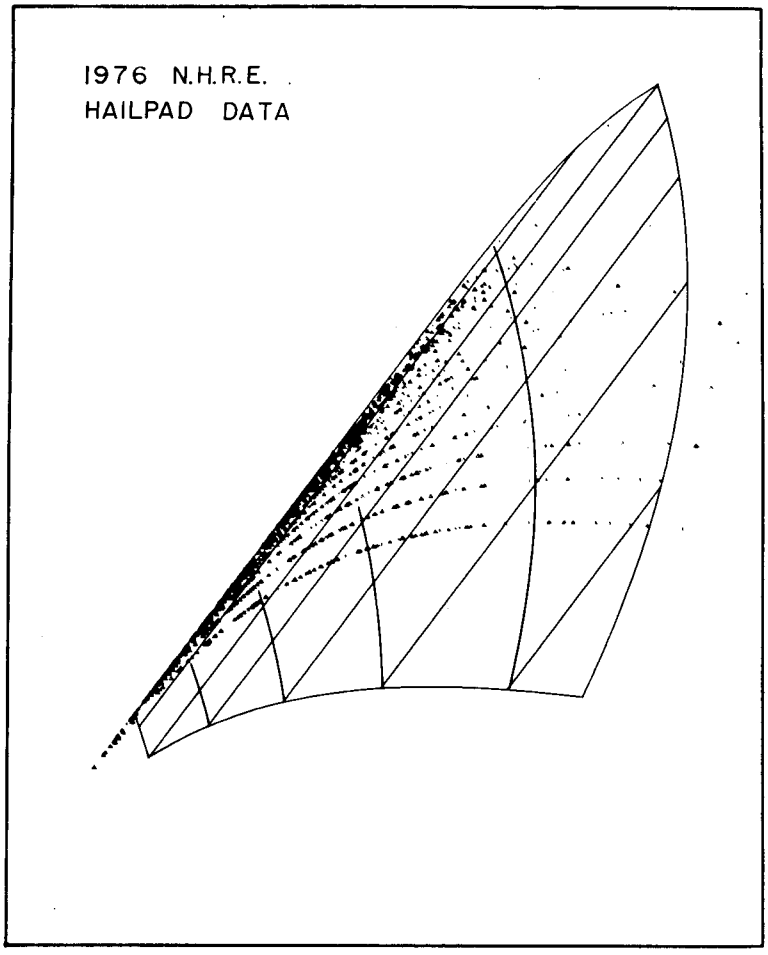

FIG. 4. Experimental hail parameters as determined from 1976 National Hail Research Experiment hailpad data plotted on the three parameter diagram. A total of 993 points is plotted on this diagram.

tion of the maximum diameter D_{max} from the hailpad data.

The hailpad data collected by the National Hail Research Experiment in 1976 in northeast Colorado have been used in a procedure like that described above and the results are plotted in Fig. 4. Each of the points was plotted using the values of Λ and D_{max} found by the method described in the Appendix. As in Fig. 3, the overwhelming majority of the data lies near the left boundary of the diagram in the region of large ΛD_{max}. Those points which lie in the region for $\Lambda D_{max} < 5$ describe images of the isopleths of D_{max} which is a reflection of the fact that the hailpad data are classified in size categories of finite width. Hence, only discrete values of D_{max} are possible corresponding to the upper bounds on each of the categories. 90% of the points lie in the region of the diagram where $\Lambda D_{max} \geqslant 5$ and 66% have $\Lambda D_{max} \geqslant 7$. Other details concerning these hailpad data and alternative methods of analysis are given in the Appendix where it is shown that the method used in arriving at these results may be considered as yielding values of ΛD_{max} which are smaller than those obtained using Eq. (17). It may therefore be concluded that for almost all meteorological situations involving hail, it is valid to approximate hailfall parameters by their large ΛD_{max} limits as found from their definitions given above. However, there is a sufficiently large number of cases in these data for which ΛD_{max} is small that the large ΛD_{max} approximations should be used with caution.

b. Radar overlays

The radar measurables considered in this work are the equivalent radar reflectivity factor Z (mm^6 m^{-3}) defined by

$$Z = \frac{\lambda^4}{\pi^5 |k|^2} \int_0^{D_{max}} N(D)\sigma_b(D)dD = \frac{10^6 \lambda^4}{\pi^5 |k|^2} \beta, \quad (18)$$

the mean Doppler fallspeed in still air $\bar{v}_T$ (m s^{-1}) given by

$$\bar{v}_T = \beta^{-1}\gamma \int_0^{D_{max}} D^{0.5}N(D)\sigma_b(D)dD \qquad (19)$$

and the variance of the Doppler spectrum σ_D^2 (cm^2) defined by

$$\sigma_D^2 = \beta^{-1}\gamma^2 \int_0^{D_{max}} (D^{0.5} - D_a^{0.5})^2 N(D)\sigma_b(D)dD, \quad (20)$$

where $|k|^2 = 0.93$ is the refractivity factor for water, $\sigma_b(D)$ (cm^2) is the backscattering cross section of a hailstone of diameter D, β is defined by the integral in Eq. (18) and λ (cm) is the radar wavelength. The diameter D_a is defined by $\bar{v}_T = \gamma D_a^{0.5}$. These definitions for $\bar{v}_T$ and σ_D^2 correspond to hail at vertical incidence.

In computing Z, $\bar{v}_T$ and σ_D^2 the backscattering cross sections of Battan *et al.* (1970) for spherical hailstones have been used. Calculations have been performed for λ = 3.21, 4.67, 5.50 and 10.0 cm and for hailstones with a thin coating of water of thickness t ranging from 0.0 to 0.5 cm. In this work only those results for λ = 3.21 and 10.0 cm and for t = 0.0, 0.01 and 0.05 cm are examined. The two conditions t = 0.0 and t = 0.01 cm are referred to here as dry hail and wet hail, respectively.

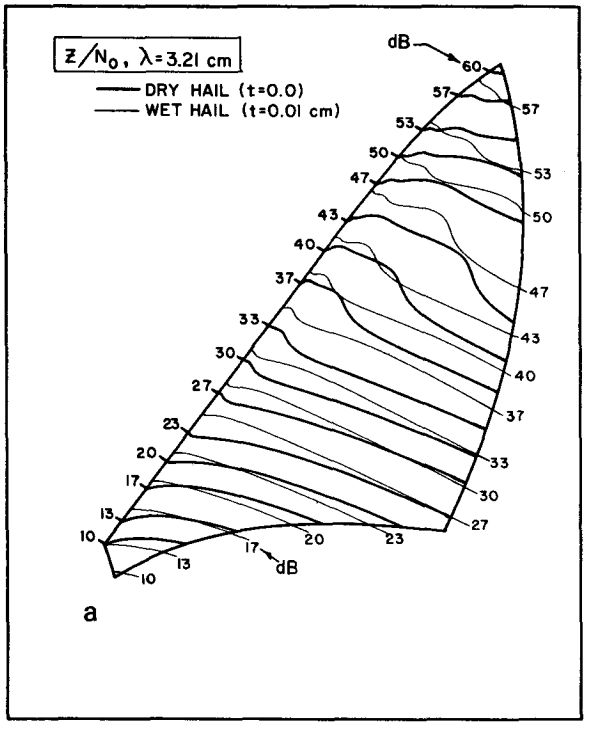

FIG. 5a. Radar overlay for three-parameter diagram showing isopleths of Z/N_0(dB) for λ = 3.21 cm and for dry hail (heavy curves) and wet hail (light curves).

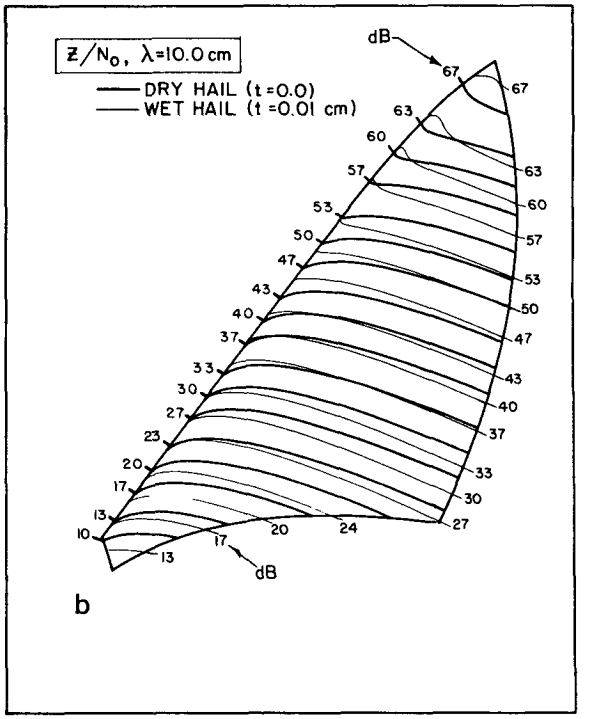

FIG. 5b. As in Fig. 5a except λ = 10.0 cm.

Isopleths of Z/N_0 are shown in Fig. 5a for λ = 3.21 cm for dry hail and wet hail. The corresponding isopleths for λ = 10.0 cm are shown in Fig. 5b. The isopleths are labeled in dB for the quantity Z/N_0, so that an isopleth bearing the label 40 dB corresponds to $\log_{10}(Z/N_0) = 4$ or $Z/N_0 = 10^4$ mm^6 cm. To convert the isopleths to dBZ for the quantity Z it is merely necessary to add 10 $\log_{10}N_0$ to the label values. For example, the average spectrum for the Federer and Waldvogel (1975) data has Λ = 4.2 cm^{-1} and $D_{max} \geq 2.0$ cm which defines a point on the hail parameter diagram through which the Z/N_0 = 33 dB wet hail isopleth passes. In addition, for this average spectrum N_0 = 121 m^{-3} cm^{-1} so that 10 $\log_{10}N_0$ = 21 and $Z \approx$ 54 dBZ which agrees very well with that found from the experimental size spectrum data for wet hail.

Calculations of equivalent reflectivity factor similar to those shown here have been performed by Atlas and Ludlam (1960) as a function of radar wavelength and maximum hailstone diameter. They display Z *versus* λ and D_{max} for dry hail (t = 0.0) and wet hail (t large, i.e., $t > 0.1$ cm) for specific values of the distribution parameters, viz., Λ = 1.3, 1.54, 1.8, 2.27 cm^{-1} and N_0 = 40 cm^{-1} over the ranges $1.8 \leq \lambda \leq 10.0$ cm and $D_{max} \leq 6.0$ cm. Although the results for large t are not shown in this work, examination of the results for dry hail in Figs. 5a and 5b for λ = 3.21 and 10.0 cm, respectively, shows that they are in excellent agreement with the Z values

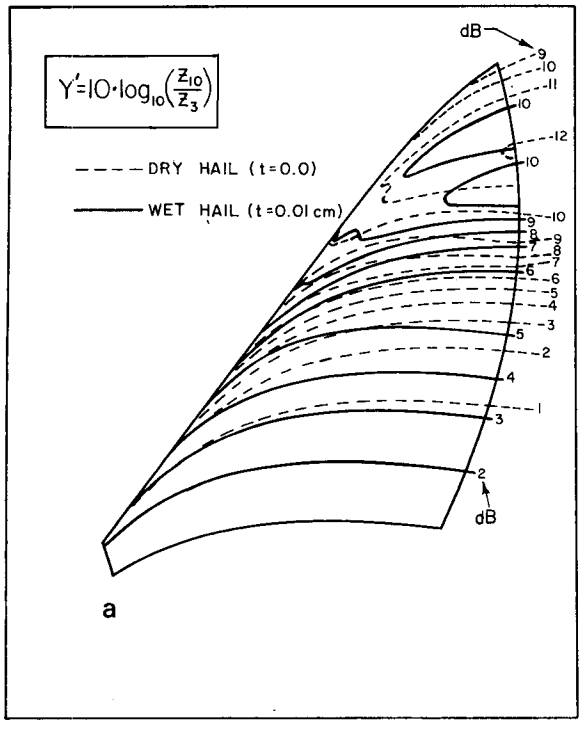

FIG. 6a. Radar overlay for three-parameter diagram showing isopleths of Z_{10}/Z_3(dB) for dry hail (dashed curves) and wet hail (solid curves). See text for further details.

found by Atlas and Ludlam (1960) for the four spectra considered by them.

Although the isopleths for dry hail in Figs. 5a and 5b are similar at small D_0's, for $D_0 \geq 1.5$ cm the $\lambda = 10.0$ cm isopleths carry labels about 10 dB greater than those for $\lambda = 3.21$ passing through the same point on the diagram. Similar remarks hold for the wet hail isopleths. This is displayed more clearly in Fig. 6a where the quantity $Y' = 10 \log_{10}(Z_{10}/Z_3)$ is plotted on the diagram, where Z_{10} and Z_3 are the reflectivity factors for $\lambda = 10.0$ and 3.21 cm, respectively. It might be concluded that this ratio would be a good measure of the size spectrum parameters; however, the isopleths in Fig. 6a possess behavior which results in ambiguity that cannot be resolved. For example, suppose that the hail is wet ($t = 0.01$ cm), $\lambda = 10.0$ cm, $Y' = 10 \log_{10}(Z_{10}/Z_3) = 10$ dB and $Z_{10}/N_0 = 60$ dB. Then the diagram shows that these data define three points for which D_0 and D_{max} can have any of the three pairs of values (1.7, 2.5 cm), (1.9, 3.0 cm) or (2.0, 3.5 cm). To unequivocally identify the spectral parameters it would be necessary to introduce a third measurable. This result has been noted by Atlas and Ludlum (1961) who attempt to infer the maximum size of hailstones produced by a storm in England from measurements of Z at three wavelengths.

Isopleths of Z/N_0 for $t > 0.01$ cm are not shown in this work; they are similar in shape to those for $t = 0.0$ and 0.01 cm in Figs. 5a and 5b. However, the quantity $Y' = 10 \log_{10}(Z_{10}/Z_3)$ for $t = 0.05$ cm is shown in Fig. 6b and the results are representative of what is found for all values of $t \geq 0.05$ cm. As in Fig. 6a, the isopleths in Fig. 6b display behavior which results in ambiguity in the values found for the size spectrum parameters. However, Figs. 6a and 6b differ in some very important respects. For example, Y' can have much larger values for $t \geq 0.05$ cm than for $t < 0.05$ cm, especially for large D_0's. In addition, there exist large areas in Fig. 6b where $Z_{10} < Z_3$ (i.e., $Y' < 0$). Extension of Fig. 6a to values of $D_{max} < 0.5$ cm would not produce values of $Y' < 0$, i.e., the ratio Z_{10}/Z_3 is always greater than one for all values of Λ and D_{max} when $t < 0.05$ cm. However, for $t \geq 0.05$ cm, $Y' < 0$ when $D_{max} \leq 1.2$ cm (or when $D_0 < 1.0$ cm). These results are in agreement with those found by Srivastava and Jameson (1977) who calculate Y' for a monodisperse spectrum and find that $Y' < 0$ for $t \geq 0.05$ cm and $0.5 < D < 1.0$ cm. They conclude as a result of these findings and other considerations that the dual-wavelength hail detection method of Eccles and Atlas (1973) is not useful for delimiting the boundaries of hail regions.

In spite of the ambiguities inherent in using Fig. 6 to deduce hailstone sizes, it is apparent that values of $Y' > 0$ are always associated with hail when $t < 0.05$ cm and $Y' < 0$ only when $t \geq 0.05$ cm and

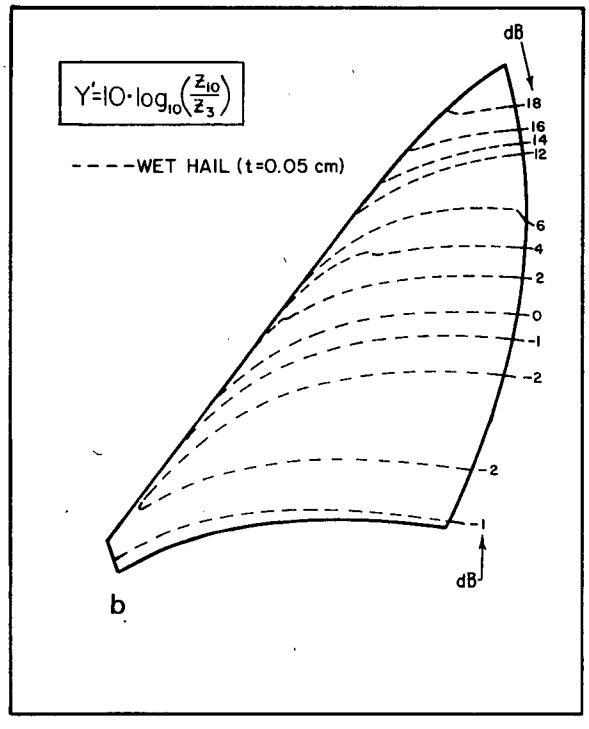

FIG. 6b. As in Fig. 6a except for wet hail with $t = 0.05$ cm.

$D_0 < 1.0$ cm (i.e., small, wet hail). This is an important result which has been employed by Jameson and Heymsfield (1980) in deducing the properties of hydrometeors in a hailstorm from dual-wavelength radar data and simultaneous aircraft penetrations. They find extensive regions in the storm where $Y' < 0$, the temperature is less than $-10°C$, and there is negligible liquid water. The results presented here are consistent with their conclusion that the hydrometeors in these regions cannot be spherical hail, dry or wet, but must be predominantly graupel and aggregates.

One of the interesting features of the isopleths in Figs. 5a and 5b is that they are roughly perpendicular to the $\Lambda D_{\max}$ isopleths in Fig. 1b. This means that Z/N_0 will be fairly insensitive to changes in $\Lambda D_{\max}$ along isopleths of the spectral parameters D_0, $\bar{D}$, $\bar{D}_m$, etc. An important consequence of this result is that within reasonable accuracy (i.e., ±2 dB) it is not necessary to specify all three parameters to determine Z. In other words, Z can be sufficiently defined from knowledge of only N_0 and one other spectral parameter, such as D_0. This has been demonstrated in the analysis of Doppler radar spectra of hail by Ulbrich (1977).

Isopleths of the mean Doppler fallspeed $\bar{v}_T$ at vertical incidence and in still air are shown in Figs. 7a and 7b for λ = 3.21 and 10.0 cm, respectively. It is immediately apparent from these figures that there is not much difference between the $\bar{v}_T$ isopleths for dry and wet hail except at $D_0 > 2.0$ cm. In addition, these isopleths show that $\bar{v}_T$ is not very sensitive to changes in $\Lambda D_{\max}$ along an isopleth of D_0 so that only one spectral parameter is needed to specify the mean Doppler fallspeed. This consequence has also been exploited in the analysis described by Ulbrich (1977) where it has been shown that there exists a simple power-law relationship between $\bar{v}_T$ and Z for hail. Consequently, measurement of Z determines $\bar{v}_T$ directly and the difference between the measured mean Doppler velocity and $\bar{v}_T$ determines the storm updraft. These points have been illustrated by Ulbrich (1977) through analysis of the vertical Doppler data of Battan and Theiss (1972) and of Strauch and Merrem (1976).

The final set of radar overlays are shown in Figs. 8a and 8b where isopleths of the variance of the Doppler spectrum σ_D^2 are shown for λ = 3.21 and 10.0 cm, respectively. These curves are very different from those shown in previous figures in that the isopleths are roughly parallel to the $D_{\max}$ isopleths in Fig. 1a. That is, the change in σ_D^2 along an isopleth of $D_{\max}$ is small whereas along an isopleth of D_0 there are large changes in σ_D^2 within the region defined by the base diagram. Closer examination of these isopleths shows that for almost all of the diagram and for both radar wavelengths considered here, $\sigma_D^2 < 2$ m^2 s^{-2} when $D_{\max} \leqslant 1.0$ cm and $\sigma_D^2 > 4$ m^2 s^{-2}

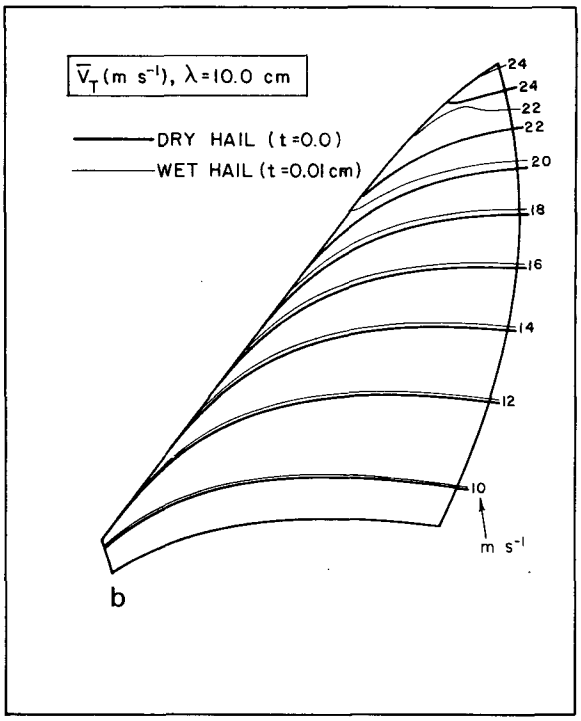

FIG. 7b. As in Fig. 7a except λ = 10.0 cm.

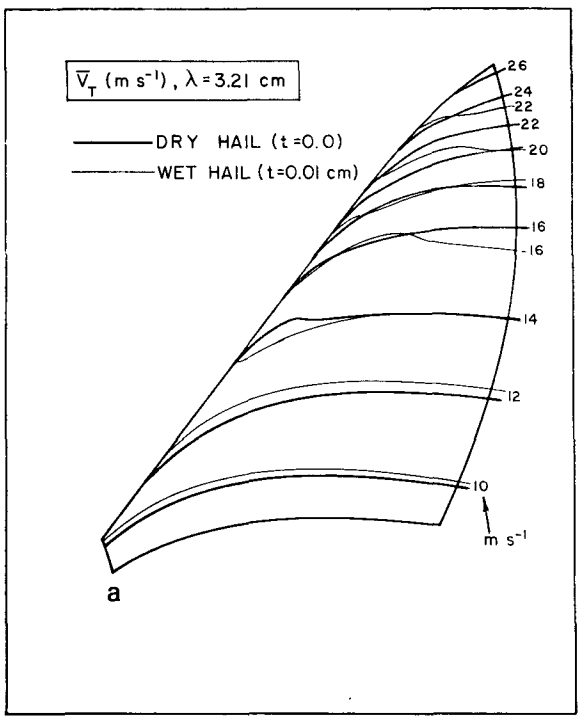

FIG. 7a. Radar overlay for three-parameter diagram showing isopleths of mean Doppler fallspeed $\bar{v}_T$ (m s^{-1}) for λ = 3.21 cm and for dry hail (heavy curves) and wet hail (light curves).

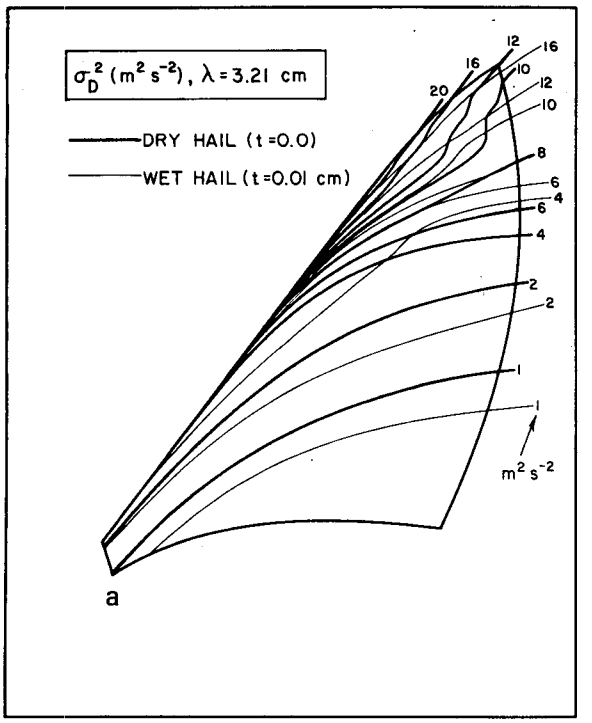

FIG. 8a. Radar overlay for three-parameter diagram showing isopleths of Doppler variance σ_D^2 (m^2 s^{-2}) for λ = 3.21 cm and for dry hail (heavy curves) and wet hail (light curves).

when $D_{max} \gtrsim 2$ cm and $D_0 \gtrsim 0.9$ cm. These results are in accord with those of Donaldson and Wexler (1969) who calculate σ_D^2 as a function of D_{max} for the single value of $\Lambda = 2.93$ cm^{-1} and for $\lambda = 3.2$, 5.4, and 10.7 cm. They compare their calculations with data for a thunderstorm which did not produce hail at the ground in New England and conclude that $\sigma_D^2 > 4$ m^2 s^{-2} indicates large hail in the radar pulse volume and $\sigma_D^2 > 2$ m^2 s^{-2} indicates small hail and/or light to moderate turbulence. However, Boston and Rogers (1969) have performed similar calculations and conclude that the influences of turbulence and shear are so strong that the Doppler variance cannot be used as a completely reliable indication of hail. Nevertheless, Z and the mean Doppler velocity are not affected by turbulence, so that their measurement at vertical incidence is sufficient to determine the distribution parameters N_0 and Λ. The value found for Λ then gives the maximum diameter D_{max} as well as the "intrinsic" Doppler variance of the particle size distribution. The difference between the measured and "intrinsic" Doppler variances therefore gives the part of the variance due to turbulence and other effects. The details of this procedure are given by Ulbrich (1977) and illustrated using the vertical Doppler data of Battan and Theiss (1972).

3. Two-parameter diagram

a. Base diagram

It has been shown in the previous section that in most cases it is appropriate to take ΛD_{max} as large. In such cases the definitions of the hail parameters given previously become much simpler. For example, Eq. (2) becomes

$$W = \pi\rho \frac{N_0}{\Lambda^4} = 0.0173\rho N_0 D_0^4, \tag{21}$$

Eq. (3) becomes

$$N_T = \frac{N_0}{\Lambda} = 0.272 N_0 D_0, \tag{22}$$

Eqs. (10)–(12) reduce to

$$E = 0.002\pi\rho\gamma^2 \frac{N_0}{\Lambda^5} = 9.4 \times 10^{-6}\rho\gamma^2 N_0 D_0^5, \tag{23}$$

$$\dot{E} = 0.00436\pi\rho\gamma^3 \frac{N_0}{\Lambda^{5.5}} = 1.07 \times 10^{-5}\rho\gamma^3 N_0 D_0^{5.5}, \tag{24}$$

$$\dot{W} = 1.94\pi\rho\gamma \frac{N_0}{\Lambda^{4.5}} = 1.75 \times 10^{-2}\rho\gamma N_0 D_0^{4.5}. \tag{25}$$

All of the above integral quantities are now functions of only two parameters, *viz.*, N_0 and D_0 which means

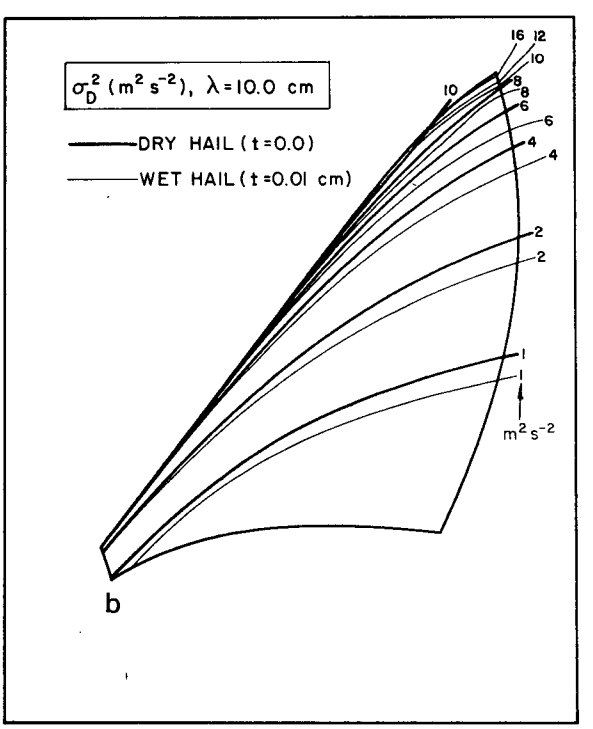

FIG. 8b. As in Fig. 8a except λ = 10.0 cm.

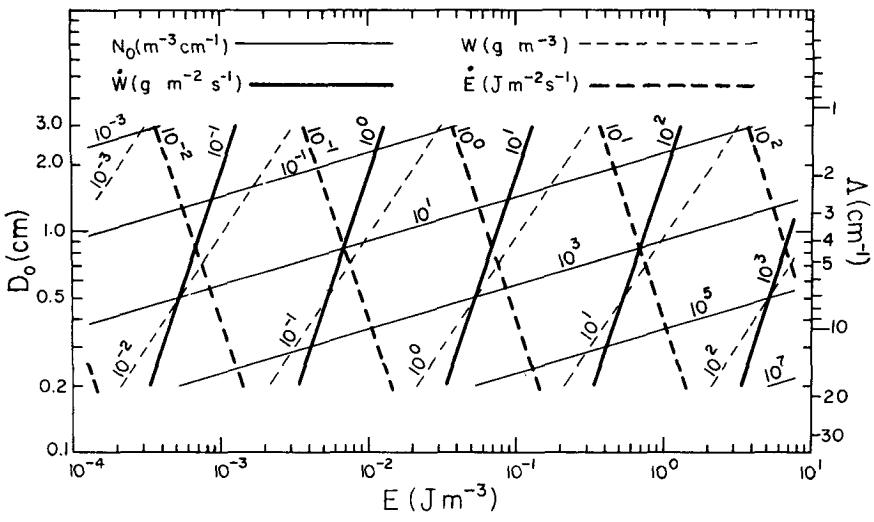

FIG. 9a. Two-parameter base diagram. Isopleths of N_0, W, $\dot{W}$ and $\dot{E}$ are shown as light solid, light dashed, heavy solid and heavy dashed lines, respectively. The units of the labels on the isopleths are shown on the diagram.

they may be represented on a two-dimensional hail parameter diagram without need for normalization as was the case in the previous section. One method of displaying the relationships among these quantities is shown in Fig. 9a which is a plot of D_0 on the vertical axis versus kinetic energy content E on the horizontal axis and with isopleths of N_0, W, $\dot{W}$ and $\dot{E}$. Note that since all of the expressions for these integral quantities involve the product of N_0 and a power of D_0, then all of the isopleths in Fig. 9a are straight lines on this log-log plot. Only those isopleths which increase by powers of 10 are shown, but because of the simplicity of the diagram it is easy to draw isopleths for intermediate values if desired. A plot of D_0 vs E has been chosen here because it produces the greatest angles between the isopleths, thus providing maximum clarity. Also shown in Fig. 9a is a scale of Λ (cm^{-1}) on the right side of the diagram corresponding to the large ΛD_{max} limit $\Lambda D_0 = 3.672$. This scale can also be transformed to a scale for any of the other spectral parameters defined earlier since they are all now functions of only Λ (or

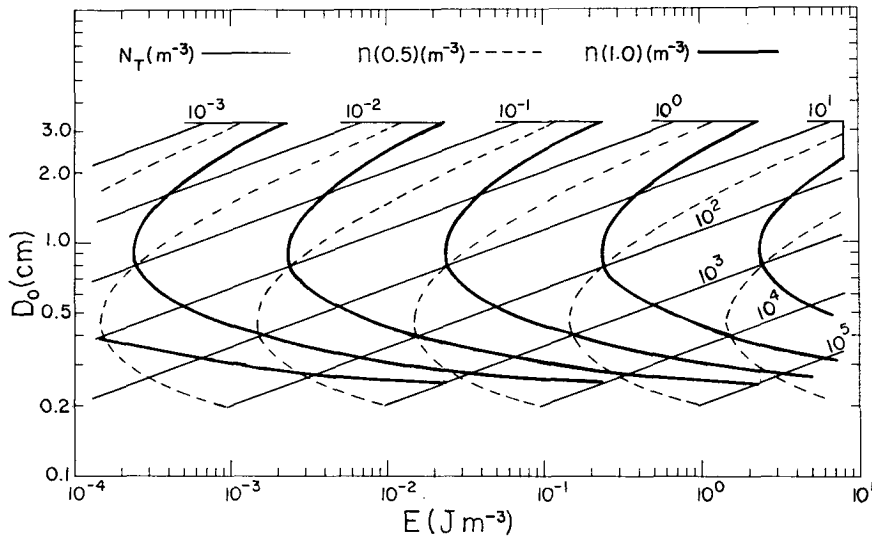

FIG. 9b. Supplement to two-parameter base diagram showing isopleths of N_T, $n(0.5)$ and $n(1.0)$ as light solid lines, dashed curves and heavy curves, respectively. The units of the labels on the isopleths are shown on the diagram.

TABLE 1. Relationships among integral hail parameters and the fractional changes in these parameters at constant liquid water content.

Relationship	Fractional change at constant W
$n(1.0) = 15.7\rho^{-1}WD_0^{-3}\exp(-3.67/D_0)$	$\frac{\delta n}{n} = \zeta^{-1}\frac{\delta D_0}{D_0}$
$E = 5.43\times10^{-4}\gamma^2 WD_0$	$\frac{\delta E}{E} = \frac{\delta D_0}{D_0} = \zeta\frac{\delta n}{n}$
$\dot{E} = 6.18\times10^{-4}\gamma^3 WD_0^{1.5}$	$\frac{\delta \dot{E}}{\dot{E}} = 1.5\frac{\delta D_0}{D_0} = 1.5\zeta\frac{\delta n}{n}$
$\dot{W} = 1.01\gamma WD_0^{0.5}$	$\frac{\delta \dot{W}}{\dot{W}} = 0.5\frac{\delta D_0}{D_0} = 0.5\zeta\frac{\delta n}{n}$
$N_T = 15.7\rho^{-1}WD_0^{-3}$	$\frac{\delta N_T}{N_T} = -3\frac{\delta D_0}{D_0} = -3\zeta\frac{\delta n}{n}$
	$\zeta = (-3 + 3.672/D_0)^{-1}$

D_0). That is, Eqs. (7)–(9) now become $\bar{D} = \Lambda^{-1}$, $\bar{D}_m = 4\Lambda^{-1}$ and $\sigma^2 = \Lambda^{-2}$, respectively. Although Fig. 9a has been constructed for $\Lambda D_{\max} \rightarrow \infty$ it is essentially unchanged for all values of $\Lambda D_{\max} > 5$.

Fig. 9b shows isopleths of N_T and $n(d)$, where $n(d)$ is the number of hailstones greater than a minimum diameter d, i.e.,

$$n(d) = \int_d^\infty N(D)dD = \frac{N_0}{\Lambda}e^{-\Lambda d}. \qquad (26)$$

The isopleths of $n(d)$ illustrate an interesting effect which occurs when modification of the hail size spectrum occurs at constant liquid water content. When Fig. 9b is overlaid on Fig. 9a and changes are considered along an isopleth of W, then it is found that reducing $n(1.0)$ (the number of hailstones > 1.0 cm) will produce a decrease in E, $\dot{E}$ and $\dot{W}$, and an increase in N_T, provided $D_0 < 1.224$ cm. For $D_0 > 1.224$ cm, a decrease in $n(1.0)$ at constant W will result in an increase in E, $\dot{E}$ and W with a concomitant decrease in N_T. These results can be demonstrated in another way using Eqs. (21)–(26). If N_0 is eliminated between Eq. (21) and each of Eqs. (22)–(26), the resultant expressions are as shown in the first column of Table 1. These expressions, in turn, imply that the fractional changes in each of these integral parameters are as shown in the second column. It is seen that $\zeta = [-3 + (3.672/D_0)]^{-1} > 0$ when $D_0 < 1.224$ cm so that $\delta n < 0$ at constant W will produce $\delta E < 0$, $\delta\dot{E} < 0$, $\delta\dot{W} < 0$ and $\delta N_T > 0$. In similar fashion, when $D_0 > 1.224$ cm, $\zeta < 0$ so that $\delta n < 0$ at constant W will result in $\delta E > 0$, $\delta\dot{E} > 0$, $\delta\dot{W} > 0$ and $\delta N_T < 0$. These results may have ramifications regarding concepts involved in seeding hailstorms to reduce the physical damage caused by hailfall.

b. *Radar overlays*

Isopleths of equivalent radar reflectivity factor Z (dBZ) are shown in Fig. 10a for $\lambda = 3.21$ cm and in Fig. 10b for $\lambda = 10.0$ cm. If isopleths are desired for values of Z or for water thicknesses and wavelengths different from those shown in Fig. 10, they can be easily generated using the large $\Lambda D_{\max}$ approximations to Z given by Ulbrich (1977) where Z/N_0 is given as a power law in D_0. However, the curves of Z/N_0 vs D_0 displayed in the latter work show slight curvature on a logarithmic plot which can be accounted by the empirical form

$$Z = \alpha N_0 D^m e^{-\epsilon D_0}. \qquad (27)$$

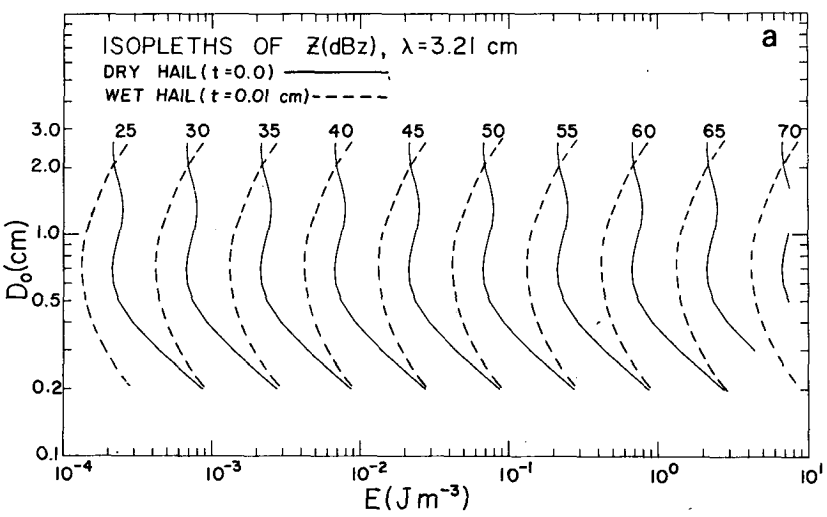

FIG. 10a. Radar overlay for two-parameter diagram showing isopleths of Z for $\lambda = 3.21$ cm and for dry hail (solid curves) and wet hail (dashed curves). The units of the labels on the isopleths are dBZ.

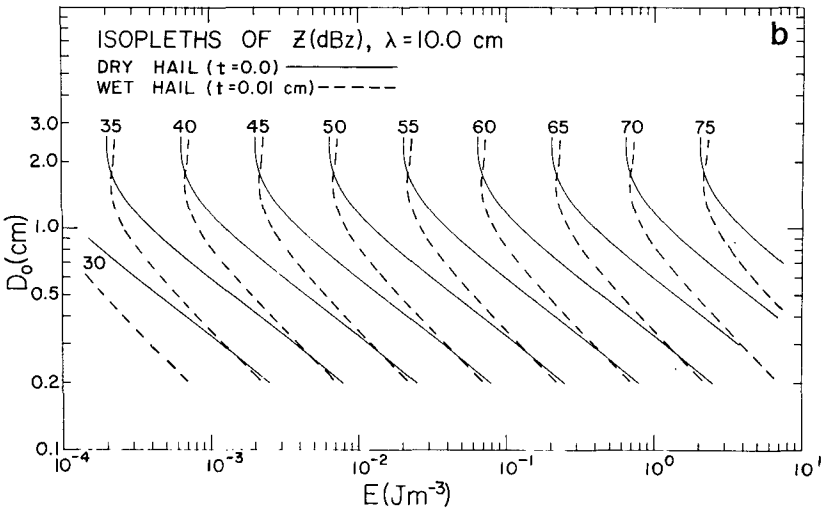

FIG. 10b. As in Fig. 10a except $\lambda = 10.0$ cm.

Eq. (27) has been fitted to the curves found by numerical integration of Eq. (18) and the results found for α, m and ϵ are given in Table 2 for $\lambda = 3.21$, 5.50 and 10.0 cm and $t = 0.0$, 0.01, 0.05 and 0.1 cm. Eq. (27) is an excellent fit to the curves found by numerical integration over the full range $t < D_0 \leq 2.6$ cm. In fact, the average deviation of this equation (without regard for sign) from any curve found from Eq. (18) with $\Lambda D_{max} \geq 5$ is less than 1 dB.

An interesting feature of the isopleths of Z in Fig. 10 is that they are roughly parallel to the isopleths of E and $\dot{E}$ for $\lambda = 3.21$ cm and are closer to being parallel to those for $\dot{E}$ for $\lambda = 10.0$ cm. The implication is that E and $\dot{E}$ are determined directly by Z so that conventional radar measurements should be sufficient to determine the kinetic energy content and flux of hailfall. In fact, it has been shown by Ulbrich (1978) that $\dot{E}$ is very closely proportional to Z at $\lambda = 3.21$ and 4.67 cm, so that at these wavelengths the relationship of $\dot{E}$ to Z is independent of fluctuations in the distribution parameter N_0. At longer wavelengths $\dot{E}$ is proportional to a power of Z less than one (i.e., $\dot{E} \propto Z^s$ where $s < 1$) so that the $\dot{E}$–Z relationship is more sensitive to N_0 fluctuations. Waldvogel *et al.* (1978a) have found similar results from an empirical analysis of hailpad data assuming Rayleigh scattering. Nevertheless, Waldvogel *et al.* (1978b) show that the results found using such an $\dot{E}$–Z relation for the total hailfall kinetic energy for large storms in Switzerland are in very good agreement with that measured at the surface by hailpads.

An application of the two-parameter diagram is shown in Fig. 11 on which D_0 is plotted versus E for more than 50 experimental hailsize distributions. These include the 28 spectra of Federer and Waldvogel (1975) and the 12 spectra of Ulbrich (1977) referred to in the previous section as well as the six spectra of Dennis *et al.* (1971) which were measured with a momentum sensor at the surface in South Dakota and the seven spectra depicted by Spahn (1976) which were measured by an airborne photoelectric particle detector in Colorado. Also shown are the N_0 isopleths and wet hail isopleths of Z for $\lambda = 3.21$ cm. The latter isopleths are shown because the spectra due to Ulbrich (1977) are deduced from the Doppler radar data of Battan and Theiss (1972) which involve a radar wavelength of 3.2 cm. In fact, these data points were plotted in Fig. 11 using the Z isopleths and the value of D_0 deduced from the experimentally measured reflectivity factor and mean Doppler velocity with the methods described by Ulbrich (1977). All other points in Fig. 11 were plotted using the values of D_0 and E calculated from the measured hail size distributions.

It is apparent that there is large scatter in these

TABLE 2. Values of constants in large ΛD_{max} approximation. $Z = \alpha N_0 D_0^m e^{-\epsilon D_0}$.*

λ (cm)	t (cm)	α	m	ϵ
3.21	0	4.67×10^3	5.97	0.629
	0.01	1.09×10^4	5.88	0.967
	0.05	1.65×10^5	6.90	2.43
	0.10	2.63×10^5	7.05	2.67
5.50	0	4.05×10^4	7.40	1.70
	0.01	1.69×10^5	6.10	0.629
	0.05	5.21×10^5	8.19	2.40
	0.10	1.49×10^6	8.68	2.99
10.0	0	2.89×10^4	7.37	0.844
	0.01	5.95×10^4	6.95	1.07
	0.05	2.71×10^4	6.39	0.234
	0.10	2.16×10^5	7.94	0.931

* Z (mm^6 m^{-3}), N_0 (m^{-3} cm^{-1}), D_0 (cm).

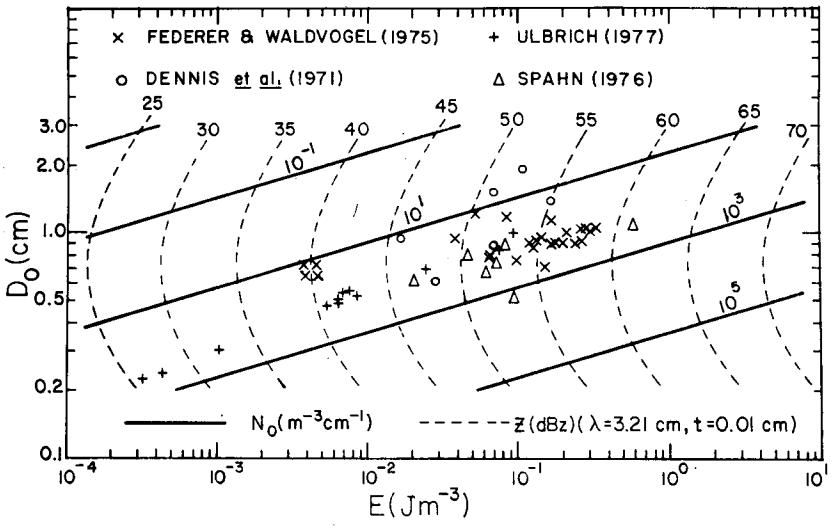

FIG. 11. Experimental size distribution parameters plotted on the two-parameter diagram. Also shown are isopleths of N_0 (heavy solid lines) and Z for λ = 3.21 cm and wet hail (t = 0.01 cm) (dashed curves). The units of the labels on the isopleths are shown on the diagram.

data. The variation in N_0 is large, ranging over more than two orders of magnitude, with most of the data falling between the $N_0 = 10^1$ and 10^3 m^{-3} cm^{-1} isopleths. This variation in N_0 is at least as large as that found for rainfall spectra and is further evidence of the need for determining at least two remote measurables to uniquely specify precipitation parameters. These points have been discussed in detail by Atlas and Ulbrich (1974) and Ulbrich and Atlas (1977, 1978) in connection with the remote measurement of rainfall parameters, and their remarks can be carried over into the present work regarding the remote measurement of hailfall parameters.

In spite of the large scatter, the data in Fig. 11 show a tendency toward a systematic variation of D_0 with E. This suggests that in those cases where only one measurable is available it is possible to obtain an estimate of hailfall parameters from the use of an empirical equation. To illustrate this the data of Federer and Waldvogel (1975) have been subjected to an empirical analysis in which relationships of the form $Z = aX^b$($X = W$, E, $\dot{W}$ or $\dot{E}$) have been determined with Z calculated for λ = 10.0 cm and t = 0.01 cm (wet hail). The resultant Z–X relationships are listed in Table 3 and are plotted on the two-parameter diagram in Fig. 12. They are in good agreement with those found by Waldvogel *et al.* (1978b) when their relations are corrected for non-Rayleigh scattering in the manner suggested by them.

All of the Z–X relations shown in Fig. 12 differ very little over the range of the diagram within which the Federer and Waldvogel data lie. These results demonstrate a point made by Atlas and Ulbrich (1974) in connection with the remote measurement of rainfall parameters, *viz.*, a relationship between any two integral parameters automatically implies all other empirical relations between all other pairs of integral parameters. In addition, such empirical relations imply other relations between the size distribution parameters N_0 and D_0. This is most easily demonstrated through an empirical analysis in which equations of the form $X = aD_0^b$ are fitted to the experimental data (where $X = W$, E, $\dot{W}$ or $\dot{E}$). The results are shown in the second column of Table 3 and are plotted in Fig. 12 where they are *all* represented by the same heavy solid straight line. The similarity of all of these X–D_0 relations is also evident from the third column in Table 3 which lists the N_0–D_0 relations deduced by substituting the empirical X–D_0 relations into the theoretical definitions in Eqs. (23), (25)–(27). There is virtually no difference among the N_0–D_0 relations in Table 2 over the range of D_0 values in the Federer and Waldvogel data.

It is apparent from the empirical relations plotted in Fig. 12 that the N_0–D_0 relation implied by all the

TABLE 3. Empirical relations derived from the data of Federer and Waldvogel (1975) and N_0–D_0 relations implied by them. Calculations involving Z assume radar wavelength λ = 10.0 cm and wet hail (t = 0.01 cm).

X	$Z = aX^b$	$X = aD_0^b$	N_0–D_0 relation implied by X–D_0 relation
W	$Z = 9.22 \times 10^5\, W^{1.23}$	$W = 1.49D_0^{4.39}$	$N_0 = 95.6D_0^{0.39}$
E	$Z = 1.32 \times 10^7\, E^{1.14}$	$E = 0.162D_0^{5.45}$	$N_0 = 98.0D_0^{0.45}$
$\dot{W}$	$Z = 4.07 \times 10^4\, \dot{W}^{1.19}$	$\dot{W} = 21.7D_0^{4.91}$	$N_0 = 98.8D_0^{0.41}$
$\dot{E}$	$Z = 6.44 \times 10^5\, \dot{E}^{1.09}$	$\dot{E} = 2.46D_0^{6.00}$	$N_0 = 93.8D_0^{0.50}$

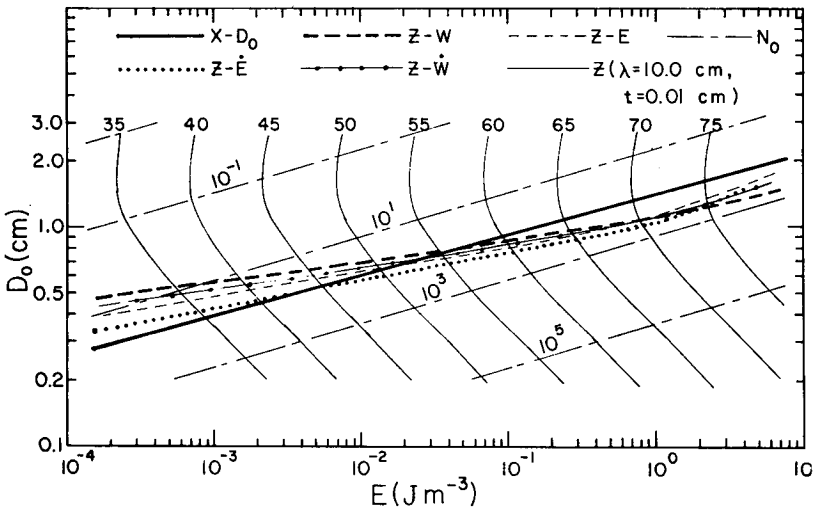

FIG. 12. Empirical relations deduced from Federer and Waldvogel (1975) data plotted on the two-parameter diagram. Also, shown are isopleths of N_0 (dot-dashed lines) and Z for $\lambda = 10.0$ cm and wet hail ($t = 0.01$ cm) (solid curves). The units of all quantities are the same as in Figs. 9 and 10.

X–D_0 relations is different from that implied by an Z–X relation. This probably is due to the fact that the Z–X analyses involve pairs of extensive integral parameters whereas the X–D_0 fits involve one integral parameter and an intensive size spectrum parameter. This indicates that an N_0–D_0 relation must be used with care in deducing size spectrum parameters.

Another application of the two-parameter diagram involves the determination of error which results when the pulse volume contains both hail and rain. In such a circumstance the measured total reflectivity factor Z_T will be given by

$$Z_T = Z_H + Z_R, \tag{28}$$

where Z_H is the equivalent reflectivity factor due to the hail in the pulse volume and Z_R is the reflectivity factor due to the rain. This can be rewritten in the form

$$Z_T = \eta Z_H, \tag{29}$$

where $\eta = 1/(1 - r)$ and r is the fractional part of the reflectivity factor due to rain, i.e., $r = Z_R/Z_T$. The variation of Z_T with Z_H, Z_R and r is shown in Fig. 13 where Z_T is plotted versus Z_H with the solid curves representing isopleths of Z_R labeled in dBZ. Also shown are isopleths of r as dashed lines labeled along the top of the diagram. Z_T deviates from the $Z_R = 0$ (no rain) isopleth by only 3 dB when $r = 0.5$, i.e., equal contributions to Z_T due to rain and hail. Along the $r = 0.1$ isopleth the difference is hardly perceived and amounts to only 0.5 dB. However, it will be shown below that the presence of rain in the pulse volume in amounts such that $r \gtrsim 0.2$ can seriously affect the values found for integral parameters such as W, E and $\dot{E}$ even though the difference between Z_H and Z_T may be small.

To show the effect on the Z isopleths of the two-parameter diagram, consider the approximate form for Z_H given by Eq. (27); using Eq. (29) above this becomes

$$Z_T = \eta \alpha N_0 D_0^{\,m} e^{-\epsilon D_0}. \tag{30}$$

Since this equation contains η simply as a multiplicative factor, the diagrams in Fig. 10 can still be used provided the Z isopleths are relabeled by adding $10 \log_{10}\eta$ to each of the labels (assuming of course that r is known). The remaining isopleths for N_0, D_0, W, E, $\dot{W}$ and $\dot{E}$ will be unaffected by such a change. The values deduced for these parameters from a measured value of Z_T will obviously be different from those found by taking $\eta = 1$ (i.e., $r = 0$, no rain) and since two quantities are required to uniquely specify a point on the diagram the effect of taking $\eta > 1$ will depend on the location along the Z isopleth. For example, dividing Eq. (21) by Eq. (30) yields

$$W = \eta^{-1} Z_T c_w D_0^{\,4-m} e^{\epsilon D_0}, \tag{31}$$

where $c_w = 0.0173\rho/\alpha$. This result shows that taking $\eta > 1$ will reduce the value found for W proportionally provided D_0 is held constant. To account for variations in D_0 it would be necessary to introduce a second measurable which would be used together with Z_T to find W.

Another approach which can be followed to estimate the effects of taking $\eta > 1$ uses the results of the empirical analysis described above. Table 3 shows that the empirical relations between Z_H and each of the integral parameters can be written in the

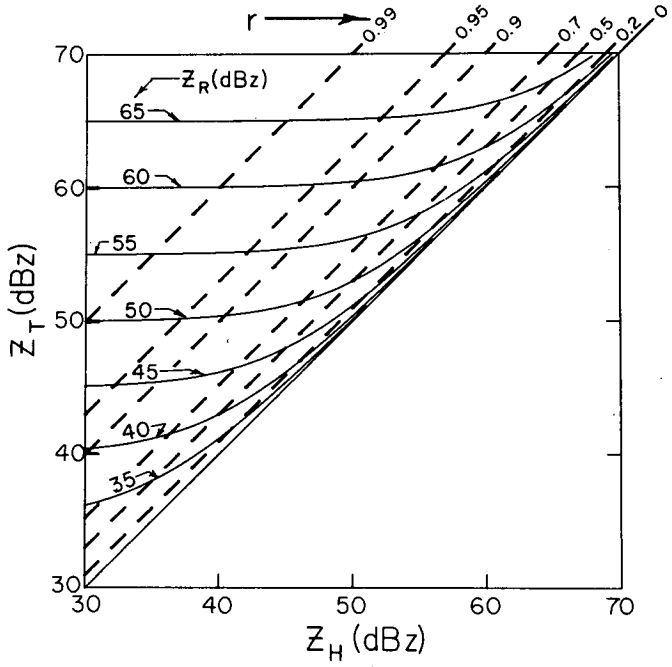

FIG. 13. Variation of total reflectivity factor Z_T with the contributions due to hail (Z_H) and rain (Z_R). Isopleths of Z_R and $r = Z_R/Z_T$ are shown as solid curves and dashed lines, respectively. The units of all quantities are shown on the figure.

form $Z_H = aX^b$, where $b = 1.23$, 1.14, 1.19 and 1.09 for $X = W$, E, $\dot{W}$ and $\dot{E}$, respectively. Substituting for Z_H using Eq. (29) and solving for the integral parameter X gives $X \propto \eta^{-\nu} Z_T^{\nu} = (1 - r)^{\nu} Z_T^{\nu}$ where $\nu = 1/b$. This means that f, the fractional difference between W as determined by taking $r = 0$ and

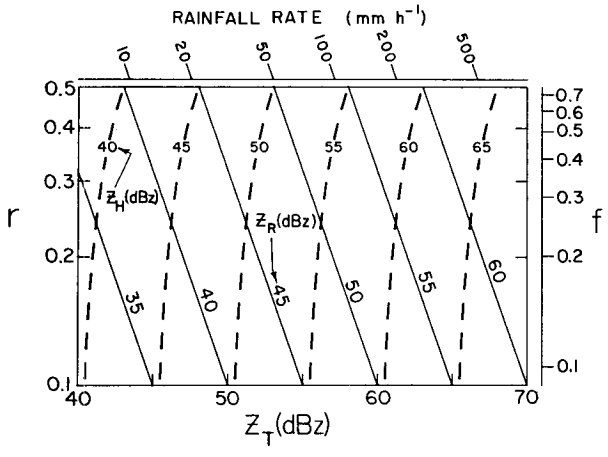

FIG. 14. Variation of Z_H and Z_R with Z_T and r, where $r = Z_R/Z_T$. Isopleths of Z_H and Z_R are shown as dashed curves and solid lines, respectively. The Z_R isopleths can be converted to rainfall rate isopleths using the scale at the top of the figure. The scale at the right gives the fractional error in W which results from neglect of the rain part of the reflectivity factor. See text for further details.

that corresponding to $r > 0$, is given by $f = (1 - r)^{-\nu} - 1$. Since $b > 1$ ($\nu < 1$) for all of the b's listed above, the value found for an integral parameter X assuming $r = 0$ will always be greater than the actual value. For example, with $X = W$, $b = 1.23$ ($\nu = 0.81$), so that a 10% contribution to Z_T due to rain ($r = 0.1$) results in an 8% overestimate in W when it is assumed that $r = 0$. When $r = 0.2$ (a 20% contribution due to rain), the assumption of no rain will result in about a 17% overestimate of W using the measured value Z_T. It is obvious that useful results will be obtained only when $r \leqslant 0.2$ or, in other words, $Z_R/Z_T \leqslant -7$ dB. Although this may at first seem to be a stringent restriction on the utility of the diagrams in this work, a closer inspection shows that in heavy hailfalls a value of $r = 0.2$ corresponds to substantial rainfall rates.

As a specific example, assume that the hailfall is described by size distribution parameters similar to those for the average spectrum observed by Federer and Waldvogel (1975), *viz.*, $N_0 \simeq 100$ m^{-3} cm^{-1} and $D_0 \simeq 1.0$ cm. Fig. 10b shows that for these parameters $Z_H \simeq 63$ dBZ so that the assumption that $r = 0.2$ means that $Z_R \simeq 56$ dBZ. Using an empirical Z_R–R relationship for thunderstorm rain of the form $Z_R = 486R^{1.37}$ [cf. Battan (1973)] it is found that for these conditions $R = 134$ mm h^{-1}. Other combinations of parameters, of course, are possible and these are depicted in Fig. 14 where r is plotted versus

Z_T with the solid straight lines and dashed curves representing isopleths of Z_R and Z_H, respectively, labeled in dBZ. The Z_R isopleths can be transformed to R isopleths using the scale at the top of the diagram. Also shown on the right of the diagram is a scale of f, the fractional difference in W as determined from Z_T with $r = 0$. Since all the b's listed above are similar, scales of f for $\dot{W}$, E and $\dot{E}$ would be very much like that shown for W in Fig. 14. This diagram shows that in heavy hailfalls ($Z_H \geqslant 60$ dBZ), acceptable levels of error ($f < 0.2$) will still permit the existence of substantial rainfall in the hailshaft.

In some large, single-cell hailstorms, spatial separation of the rain and hail at the surface has been observed. For example, Browning (1964) has reported surface observations for a storm in Oklahoma for which the hail fell from the intense echo surrounding the weak echo vault while the rain fell ahead of this region on the storm's left forward quadrant. The analysis of surface precipitation data by Foote and Fankhauser (1973) for a hailstorm in Colorado displays similar displacement of the hailswath from the region of most intense rainfall. If it is possible in these large hailstorms to distinguish between those parts of the radar echo which are rain and hail, then the results presented here can be applied directly to the hail signal. Methods by which such a distinction could be made might include the dual-measurement techniques surveyed by Srivastava and Jameson (1977) or the use of the ratio of the reflectivity factors Z_{10} and Z_3 as recommended by Jameson and Srivastava (1978). If, after such delineation of the hailbearing regions, it is believed that they contain a mixture of rain and hail, then the rainfall rate in regions adjacent to the hailshaft can be used to estimate r from which the expected error in integral parameters can be deduced using the methods described above. In any event, the measurements by Waldvogel *et al.* (1978a) of rainfall and hailfall at the surface for a large storm in Switzerland show that $r < 0.1$ for almost the full duration of hailfall at the measurement site. Furthermore, Auer and Marwitz (1972) found $r \simeq 0$ in 40 aircraft encounters with hail at cloud base in the updrafts of 15 storms in Alberta and Colorado. These results suggest that the diagrams presented here can be used for analysis of the radar signal from a hailshaft without application of a correction for the part of the reflectivity factor due to rain.

Given the fact there are at present no unequivocal remote hail signatures, it is unlikely that it would be possible to clearly and reliably distinguish hailshafts from regions of rain such as those discussed above for supercell storms. In addition, Dye and Martner (1978) have shown that for Colorado hailstorms it is not even possible to define a reflectivity threshold which separates rain from hail. Nevertheless, Waldvogel *et al.* (1978a) have devised a multiple regression technique, based on both radar and hailpad measurements, to compute the kinetic energy of hail reaching the surface. When the technique is applied to storms in Switzerland to compute the "global" kinetic energy (i.e., that for the entire storm), they find standard deviations of 20% between the values measured by the radar and the hailpad network. While they note that it is not necessary to know the exact contributions of rain and hail to the total reflectivity, it is implicit in their method that on the average the contribution by rain is some fraction of that due to hail at each reflectivity value. While the results obtained in Switzerland are promising, their generality remains to be determined. Clearly, there is need for a great deal more data in various regions of the world.

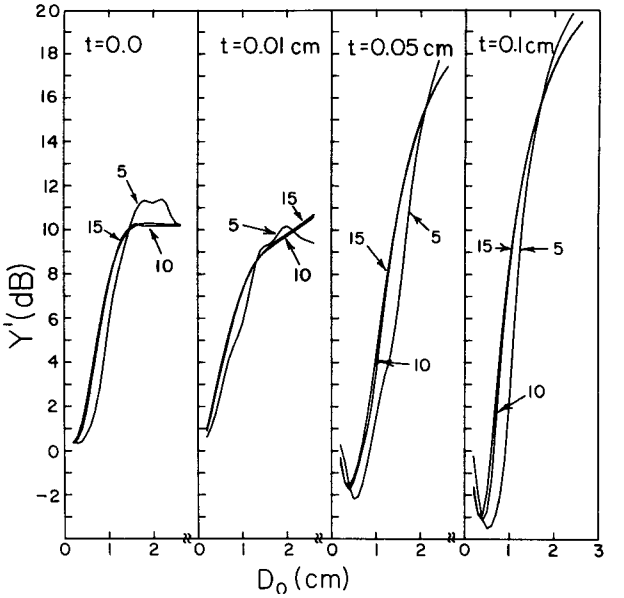

FIG. 15. $Y' = 10 \log_{10}(Z_{10}/Z_3)$ vs D_0 for values of $\Lambda D_{max} = 5$, 10, 15 and water thicknesses $t = 0.0$, 0.01, 0.05, 0.1 cm. Each curve is labeled with the value of ΛD_{max} to which it corresponds.

As a final example of the use of the two-parameter distribution, consider the variation of $Y' = 10 \log_{10}(Z_{10}/Z_3)$ with D_0. The dependence of Y' on the three-parameter distribution was discussed in the previous section and illustrated in Fig. 6. In the limit of large ΛD_{max} this quantity is insensitive to changes in ΛD_{max}. This is illustrated in Fig. 15 where Y' is plotted versus D_0 for values of $\Lambda D_{max} = 5$, 10, 15 and for water thicknesses $t = 0.0$, 0.01, 0.05, 0.1 cm. It is apparent that Y' is very closely a function of D_0 only when $\Lambda D_{max} > 5$. It is also obvious that Y' increases sharply as t increases when $D_0 > 1.5$ cm. It is unlikely, however, that such large values of Y' would be observed since they correspond to unreasonably large values of Z_{10}. To demonstrate that such

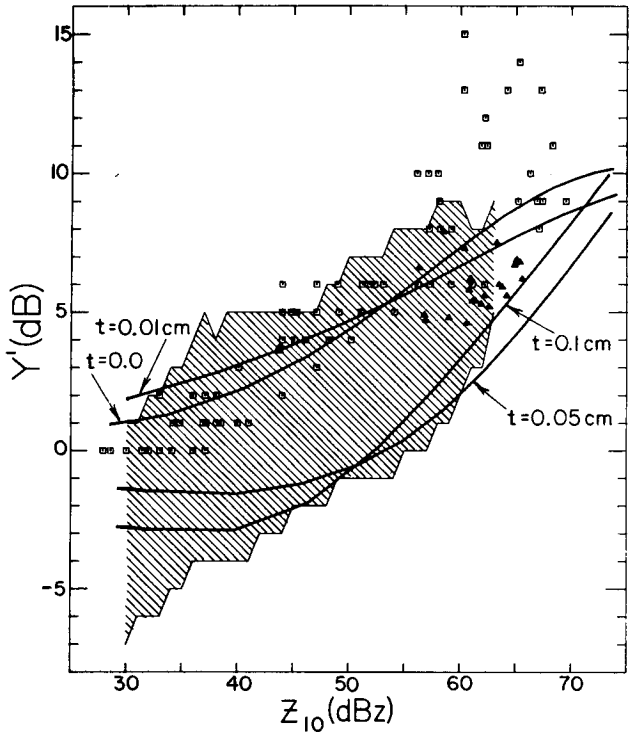

FIG. 16. $Y' = 10 \log_{10}(Z_{10}/Z_3)$ vs Z_{10} for values of water coating thicknesses t = 0.0, 0.01, 0.05, 0.1 cm and with N_0 = 100 m^{-3} cm^{-1} (heavy solid curves). Also shown as a shaded portion of the figure is the region within which lies 90% of the observations of Jameson and Heymsfield (1980). The squares are the data of Dennis *et al.* (1971), and the triangles are points calculated from the data of Federer and Waldvogel (1975).

is the case, plots of Y' vs. Z_{10} are shown in Fig. 16 as heavy solid curves for the four values of t listed above. In constructing this diagram the large ΛD_{max} behavior of Y' and of Z_{10}/N_0 have been used and points corresponding to the same D_0 have been plotted and connected by line segments. It has been assumed in plotting Z_{10} that N_0 = 100 m^{-3} cm^{-1}; smaller or larger values of N_0 will merely shift the curves to the left or right, respectively, since Y' is independent of N_0. Comparison of this figure with Fig. 15 shows that observation of values of Y' in excess of 10 dB would require large t, exceedingly large values of Z_{10} and/or very small values of N_0; these conditions have not been observed in nature. Also shown in Fig. 16 is the shaded region plotted by Jameson and Heymsfield (1980) within which 90% of their observations lie. In addition, the data of Dennis *et al.* (1971) are shown plotted as squares and the results found by calculating Y' and Z_{10} from the experimental spectra of Federer and Waldvogel (1975) are plotted as triangles. Although all of these results could be accounted for by a variety of t's and N_0's, the calculated curves and the experimental data are in agreement with the conclusions of Jameson and Heymsfield (1980) regarding criteria for the presence of hail. If the hail is dry or covered with a very thin coat of water $Y' > 3$ dB only when $Z_{10} \geqslant 45$ dBZ. Thicker coats of water require that $Z_{10} > 60$ dBZ to observe $Y' = 3$ dB. Consequently, the criterion that $Y' \geqslant 3$ dB for hail will include only those cases for large t when Z_{10} is large, thereby avoiding any interpretation of signals from regions with graupel as being hail-bearing.

4. Summary and conclusions

Two extensive sets of diagrams have been presented in this work which depict the relationships among hail-size distribution parameters and integral quantities defined in terms of these parameters. The first set of diagrams employs a truncated exponential three-parameter size distribution of the form $N(D) = N_0 \exp(-\Lambda D)$, $0 \leqslant D \leqslant D_{max}$ and has been used to deduce conclusions regarding the relationships between integral quantities and remote measurables. Generally, since $N(D)$ is dependent on three parameters, three measurables would be required to completely specify the size distribution and derived integral quantities. However, it has been shown that integral parameters such as equivalent radar reflectivity factor are insensitive to changes in the product ΛD_{max} for values of $\Lambda D_{max} > 5$. It has also been shown that the overwhelming majority of experimentally measured size distributions have $\Lambda D_{max} > 5$ so that in most cases the product of Λ and the median volume diameter D_0 approaches its limiting value of $\Lambda D_0 = 3.672$. This means that only two size distribution parameters (e.g., N_0 and D_0) are adequate to specify accurately most integral quantities. A further consequence is that only two remote measurables are required to determine accurately most integral quantities when the contribution due to rain can be neglected.

The three-parameter diagrams have been used in several other ways in this work. For example, it has been shown that the mass-weighted average diameter $\bar{D}_m$ is always within 10% of the median volume diameter D_0 which is a useful result for the analysis of hail-size spectral data. The behavior of Y', the ratio of the reflectivities at λ = 10.0 and 3.2 cm, as a function of Λ, D_{max} and D_0 has been examined and its use by Jameson and Heymsfield (1980) as an indicator of hail size or the presence of graupel has been supported. Doppler-radar parameters such as mean Doppler fallspeed and Doppler variance have also been examined. The validity of the analytical techniques used by Ulbrich (1977) to deduce hail size from Doppler-radar spectra has been established. In addition, the behavior of the Doppler variance has been shown to be such that values in excess of 4 m^2 s^{-2} imply large hail and/or turbulence, in agreement with the conclusions of Donaldson and Wexler (1969) and Boston and Rogers (1969).

The second set of diagrams employs the empirical result found in the first part of the paper, *viz.*, that the product ΛD_{max} is large. Consequently, this set of diagrams involves a two-parameter size distribution and is valid for the great majority of naturally occurring hail-size distributions. These diagrams have been used to show that at certain radar wavelengths the relationship between kinetic energy flux $\dot{E}$ and radar reflectivity factor Z is such that $\dot{E}$ is directly determined from measurements of Z when the contribution due to rain is small. In other words, only one measurable is needed in this case to adequately specify an integral quantity. The diagram has been used to show that modification of the hail-size spectrum at constant ice water content (through a change in hail size and/or number) can, in some circumstances, result in either an increase or decrease in the number of hailstones > 1.0 cm, depending on how the modification is accomplished. The implication of these results in terms of the physical damage caused by hailfall is not known because of the lack of adequate information concerning hail damage functions.

The two-parameter diagram has also been used to assess the error which can be expected when the radar pulse volume contains a mixture of rain and hail. It has been found that integral hail parameters can be measured remotely by radar with acceptable levels of accuracy when the rain part of the reflectivity factor is <20% of the total.

Finally, an investigation has been made of the theoretical dependence of Y' on median volume diameter, water coat thickness and reflectivity factor at radar wavelength of 10.0 cm in the large ΛD_{max} limit. It has been shown that, for $\Lambda D_{max} > 5$, Y' is a function of D_0 only if t is known. In addition, the behavior of Y' as a function of Z_{10} is in agreement with the experimental observations and supports the criteria used by Jameson and Heymsfield (1980) for the presence of hail.

These are only a few of the possible applications of the diagrams presented in this work and the conclusions which can be drawn from them. They illustrate how the diagrams can be applied to a wide variety of situations defined by the special needs and interests of the reader. In future work it will be shown how to use these diagrams for size distributions other than exponential. Two specific types of size distributions which will be considered in this regard are the rectangular distribution and the gamma distribution of Khrgian *et al.* (1952). It will be shown that for these distributions and *for any others* for which the moments of the distribution are known, the diagrams in Section 3 can be used as shown provided the isopleths are relabeled with values appropriate to the size distribution of interest using simple multiplicative factors.

Acknowledgments. The authors express their appreciation to two J.A.M. reviewers whose comments helped to make important improvements in the manuscript. Copies of the diagrams presented in this work can be obtained from the authors. One of the author's (CWU) participation in this work was supported in part by grant ATM-7807789 to Clemson University from the Meteorology Program, Division of Atmospheric Sciences, National Science Foundation.

APPENDIX

Analysis of 1976 National Hail Research Experiment Hailpad Data

The hailpad data collected during the summer of 1976 by the National Hail Research Experiment (NHRE) consist of numbers of dents of specified size in 12-inch square styrofoam hailpads covered with aluminum foil. All dents in the pads were measured and then categorized so that if x_i (mm) is the dent dimension at the center of the ith category and Δx_i (mm) is the width of the category, then

$$\left.\begin{aligned} x_1 &= 3.5 \text{ mm} \qquad \Delta x_1 = 3.0 \text{ mm} \\ x_i &= i + 3.5 \text{ mm} \qquad \Delta x_i = 1.0 \text{ mm} \\ & \qquad i = 2, 3, \ldots, 21 \\ x_i &= 5i - 82.5 \text{ mm} \qquad \Delta x_i = 5.0 \text{ mm} \\ & \qquad i = 22, \ldots, 25 \end{aligned}\right\} \quad \text{(A1)}$$

These category dimensions are transformed to dimensions of equivalent hailstone diameters through the use of the calibration equation

$$D_i \text{ (mm)} = (a_1 x_i + a_2)^{1/2} - a_3 , \qquad \text{(A2)}$$

where the a_1, a_2, and a_3 are empirically determined constants.

The quantities of interest in this work are the volume distribution of hailstones and the maximum diameter hailstone striking the pad. If $n(D_i)$ is the number of hailstones in the ith category then the volume distribution is given by

$$N(D_i) = n(D_i)/(A\gamma D_i^{1/2} \Delta t \Delta D_i), \qquad \text{(A3)}$$

where A is the area of the hailpad, Δt is the time duration of hailfall on the pad, and ΔD_i is the width of the equivalent diameter category [found from Eq. (A2)]. Following Waldvogel *et al.* (1978a), the fallspeed of the hailstones has been taken to be of the form $v(D_i) = \gamma D_i^{0.5}$ with $\gamma = 13.96$ m s^{-1} cm$^{-0.5}$. Since the time interval Δt is not known, $N(D_i)$ cannot be determined except within a multiplicative constant. Nevertheless, if the data are approximated by an exponential form, i.e.,

$$N(D_i) = N_0 e^{-\Lambda D_i}, \qquad \text{(A4)}$$

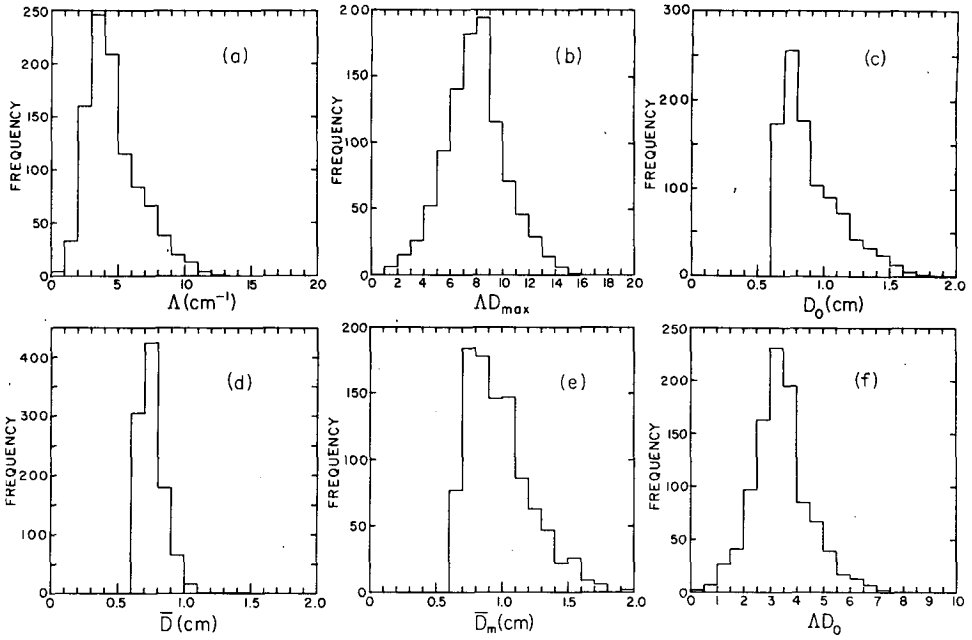

FIG. 17. Frequency distributions of hail size distribution parameters for 1976 NHRE hailpads. Parts a–f correspond to distributions for Λ, ΛD_{max}, D_0, $\bar{D}$, $\bar{D}_m$, and ΛD_0, respectively.

then it is still possible to determine the parameter Λ since only the constant N_0 depends on Δt. Eq. (A4) has been fitted to the data for each hailpad having numbers of hailstones greater than zero in four or more categories. This criterion was satisfied for 993 hailpads in the 1976 NHRE data and the frequency distribution of values found for Λ is shown in Fig. 17a. The distribution is sharply peaked about the mean value $\Lambda = 4.67$ cm^{-1} with 74% of the points lying in the range $2 \leqslant \Lambda < 6$ cm^{-1}. The maximum diameter D_{max} was estimated from the upper bound of the highest equivalent diameter category within which there were hailstones striking the pad. From this the product ΔD_{max} was formed and the resultant frequency distribution of values for this quantity is shown in Fig. 17b. This figure illustrates in a different way the result shown in Fig. 4 of the text, viz., for the overwhelming majority of the points the product ΛD_{max} is large. The average value of the distribution in Fig. 17b is $\Lambda D_{max} = 7.9$ with 90% of the points having $\Lambda D_{max} \geqslant 5$ and 66% having $\Lambda D_{max} \geqslant 7$. Another method of determining ΛD_{max} is described in the text wherein the ratio W/N_T is calculated from the hailpad data and set equal to the function on the right side of Eq. (17). Using the value found for Λ from a semi-logarithmic plot of the hailpad data, the product ΛD_{max} is then found from the solution of Eq. (17). The results found in this way for the 1976 NHRE hailpad data produce values for ΛD_{max} such that 90% of them have $\Lambda D_{max} > 10$.

The median volume diameter D_0, the average diameter $\bar{D}$ and the mass-weighted average diameter $\bar{D}_m$ also were calculated for each hailpad and the resultant frequency distributions are shown in Figs. 17c–17e. The D_0 distribution has an average value of 0.908 cm with 72% of the points lying in the range $0.6 \leqslant D_0 < 1.0$ cm. The $\bar{D}$ distribution is even more sharply peaked with an average value of 0.761 cm and 91% of the points lying between $0.6 \leqslant \bar{D} < 0.9$ cm. The $\bar{D}_m$ distribution is similar to that for D_0 with an average value of $\bar{D}_m$ equal to 0.982 cm and with two-thirds of the points in the range $0.7 \leqslant \bar{D}_m < 1.1$ cm. These frequency distributions demonstrate the point made in the text that $\bar{D}_m$ is a close approximation to D_0 for a truncated exponential distribution. If the hailpad size distributions were truly exponential then $\bar{D}_m/D_0 = 1.09$ when ΛD_{max} is large. From the results given here one finds a value of 1.08 for the ratio of the average values of $\bar{D}_m$ and D_0.

The product ΛD_0 was formed from the results found for Λ and D_0 and the frequency distribution of ΛD_0 values is shown in Fig. 17f. It is sharply peaked around the average value of 3.91 with 70% of the points lying in the range $2.5 \leqslant D_0 < 4.5$. This average value is close to that expected for a large ΛD_{max} continuous exponential distribution, i.e., $\Lambda D_0 = 3.672$.

REFERENCES

Atlas, D., 1953: Optical extinction by rainfall. *J. Meteor.*, **10**, 486–488.

——, and F. Ludlam, 1960: Multi-wavelength radar reflectivity of hailstorms. Tech. Rep. No. 4, Contract AF 61(052)-254, Dept. Meteor., Imperial College of Science and Technology, London, 96 pp.

——, and ——, 1961: Multi-wavelength radar reflectivity of hailstorms. *Quart. J. Roy. Meteor. Soc.*, **87,** 523–534.

——, and C. W. Ulbrich, 1974: The physical basis for attenuation-rainfall relationships and the measurement of rainfall parameters by combined attenuation and radar methods. *J. Rech. Atmos.*, **8,** 275–298.

Auer, A. H., Jr., and J. D. Marwitz, 1972: Hail in the vicinity of organized updrafts. *J. Appl. Meteor.*, **11,** 748–752.

Battan, L. J., 1973: *Radar Observation of the Atmosphere.* University of Chicago Press, 324 pp.

——, S. R. Browning and B. M. Herman, 1970: Tables of the radar cross sections of dry and wet ice spheres. Tech. Rep. No. 21, Inst. Atmos. Phys., University of Arizona, Tucson, 11 pp.

——, and J. B. Theiss, 1972: Observed Doppler spectra of hail. *J. Appl. Meteor.*, **11,** 1001–1007.

Boston, R. C., and R. R. Rogers, 1969: Hail detection by Doppler radar. *J. Appl. Meteor.*, **8,** 837–840.

Browning, K. A., 1964: Airflow and precipitation trajectories within severe local storms which travel to the right of the winds. *J. Atmos. Sci.*, **21,** 634–639.

Dennis, A. S., and D. H. Musil, 1973: Calculations of hailstone growth and trajectories in a simple cloud model. *J. Atmos. Sci.*, **30,** 278–288.

——, P. L. Smith, Jr., G. A. P. Peterson and R. D. McNeil, 1971: Hailstone size distributions and equivalent radar reflectivity factors computed from hailstone momentum records. *J. Appl. Meteor.*, **10,** 79–85.

Donaldson, R. J., Jr., and R. Wexler, 1969: Flight hazards in thunderstorms determined by Doppler velocity variance. *J. Appl. Meteor.*, **8,** 128–133.

Douglas, R. H., 1963: Size distributions of Alberta hail samples. Sci. Rep. MW-36, Stormy Weather Research Group, McGill University, Montreal, 55–70A.

Dye, J. E., and B. E. Martner, 1978: The relationship between radar reflectivity factor and hail at the ground for northeast Colorado thunderstorms. *J. Appl. Meteor.*, **17,** 1335–1341.

Eccles, P. J., and D. Atlas, 1973: A dual-wavelength radar hail detector. *J. Appl. Meteor.*, **12,** 847–854.

English, M., 1973: Alberta hailstorms, Part II: Growth of large hail in the storm. *Meteor. Monogr.*, No. 36, Amer. Meteor. Soc., 37–98.

Federer, B., and A. Waldvogel, 1975: Hail and raindrop size distributions from a Swiss multicell storm. *J. Appl. Meteor.*, **14,** 91–97.

——, and ——, 1978: Time-resolved hailstone analyses and radar structure of Swiss storms. *Quart. J. Roy. Meteor. Soc.*, **104,** 69–90.

Foote, G. B., and J. C. Fankhauser, 1973: Airflow and moisture budget beneath a northeast Colorado hailstorm. *J. Appl. Meteor.*, **12,** 1330–1353.

Gertzman, H. S., and D. Atlas, 1977: Sampling errors in the measurement of rain and hail parameters. *J. Geophys. Res.*, **82,** 4955–4966.

Jameson, A. R., and R. C. Srivastava, 1978: Dual-wavelength Doppler radar observations of hail at vertical incidence. *J. Appl. Meteor.*, **17,** 1694–1703.

——, and A. J. Heymsfield, 1980: Hail growth mechanisms in a Colorado storm. Part I. Dual-wavelength radar observations. *J. Atmos. Sci.*, **37,** 1763–1778.

Khrgian, A. K. A., I. P. Mazin and V. Cao, 1952: Distribution of drops according to size in cloud. *Tr. Tsentr. Aerol. Obs.*, **7,** 56.

Marshall, J. S., and W. McK. Palmer, 1948: The distribution of raindrops with size. *J. Meteor.*, **5,** 165–166.

Rinehart, R. E., 1975, National Center for Atmospheric Research, personal communication.

Spahn, J. F., 1976: The airborne hail disdrometer: An analysis of its 1975 performance. Rep. 76-13, Inst. Atmos. Sci., South Dakota School of Mines and Technology, Rapid City, 65 pp.

Srivastava, R. C., and A. R. Jameson, 1977: Radar detection of hail. *Meteor. Monogr.*, No. 38, Amer. Meteor. Soc., 269–277.

Strauch, R. G., and F. H. Merrem, 1976: Structure of an evolving hailstorm Part III: Internal structure from Doppler radar. *Mon. Wea. Rev.*, **104,** 588–595.

Ulbrich, C. W., 1974: Analysis of Doppler radar spectra of hail. *J. Appl. Meteor.*, **13,** 387–396.

——, 1977: Doppler radar relationships for hail at vertical incidence. *J. Appl. Meteor.*, **16,** 1349–1359.

——, 1978: Relationships of equivalent reflectivity factor to the vertical fluxes of mass and kinetic energy of hail. *J. Appl. Meteor.*, **17,** 1803–1808.

——, and D. Atlas, 1977: A method for measuring precipitation parameters using radar reflectivity and optical extinction. *Ann. Telecomm.*, **32,** 415–421.

——, and D. Atlas, 1978: The rain parameter diagram: methods and applications. *J. Geophys. Res.*, **83,** 1319–1325.

Waldvogel, A., W. Schmid and B. Federer, 1978a: The kinetic energy of hailfalls. Part I: Hailstone spectra. *J. Appl. Meteor.*, **17,** 515–520.

——, B. Federer, W. Schmid and J. F. Mezeix, 1978b: The kinetic energy of hailfalls. Part II: Radar and hailpads. *J. Appl. Meteor.*, **17,** 1680–1693.

Weber, S. F., 1976: The D_m analysis of precipitation particle size distributions. Rep. 76-14, Inst. Atmos. Sci., South Dakota School of Mines and Technology, Rapid City, 79 pp.